

Title: Aerosol chemistry, transport and climatic implications during extreme biomass burning emissions over Indo-Gangetic Plain  
MS No.: acp-2018-446

Authors sincerely appreciate the careful reviews and suggestions provided by the reviewer and thank the reviewer and the Editor for their time to evaluate the manuscript. Authors have made appropriate changes to the manuscript in response to the comments that have considerably improved the manuscript. In authors' response, authors have responded point-by-point to comments (reviewer comments in *blue*, authors' responses in *black*), and have included the revisions in the text with and without tracked-changes.

### Authors' Responses to Referee # 1

Singh et al. analyse the effects of biomass burning on aerosol distribution, chemistry, and radiative forcing over the Indo-Gangetic Plain combining in situ and satellite-based observations and radiative transfer calculations. Manuscript can be considered for publication in ACP however several comments should be addressed.

1. Page 1, l.36: "weighted of air trajectories" to "weighted air trajectories"  
Modified in the revised text.
2. Page 1, l.41: "must need to be studied" to "are needed"  
The sentence has been modified (page 1, l.39-41).
3. Page 1, l.42: "in much finer scale to improve parameterization of aerosol/-climate model across the region."  
This is not clear. Rewrite or remove.  
Authors emphasized that such detailed characterization of aerosol chemistry over IGP will be useful for reducing uncertainties in regional aerosol-climate model. However, as suggested, authors have modified the text (page 1, l.39-41).
4. Page 4, l.10: wunderground.com data is validated with regional weather monitoring station data! Why is that needed, and how good the validation results turned out to be?  
To understand the implications of meteorology on particulate mass, daily mean of meteorological variables was required. The regional weather monitoring station, as maintained by India Meteorological Department (IMD), is although located close to the particulate sampling station however, only reports daily maximum (at 1730 h) and daily minimum (at 0830 h). To be accurate, authors have considered daily means from wunderground.com (WU), which reports weather data collected directly from automated weather stations operating at airports (here in Babatpur, Varanasi). The aerial distance of Varanasi airport to particulate monitoring station is 23 km. We therefore, compared daily maximum and minimum (as reported by IMD) against WU reported observations and found no significant difference. Likewise, WU reported daily maximum ( $R^2$ : 0.955) and minimum temperature ( $R^2$ : 0.964) was found well validated against IMD reported observations.
5. Page 4, l.13: What is meant by simulated meteorological observations?  
This was in context of ABL height (at 0.5°) which was retrieved from NCEP's Global Data Assimilation System (GDAS). The GDAS is the system used by the NCEP Global Forecast System (GFS) model to place observations from individual station into a gridded model. GDAS adds meteorological observations like surface observations, balloon data, wind profiler data, aircraft reports etc. from a station to simulate a gridded, 3-D, model space available at various resolutions.
6. Page 4, l.14: "measure" to "analyze" in context of NCEP data.

Modified in the revised text (Page 4, l.14).

7. Page 8, l.12: “OPAC derived outputs were tuned in respect to measured relative humidity”. This is not clear. OPAC outputs are for different humidity ranges. How could output be tuned further! clarify / rewrite.  
Authors admit the error and deleted the text from the revised manuscript (Page 8, l.14). Authors wish to mention that the OPAC derived outputs (AOD and SSA) are reconstructed in a way so the modelled (OPAC output) and observed/satellite derived values matches within  $\pm 5\%$  deviation. Average relative humidity for dominating period (RH: 70%) and for non-dominating period (RH: 80%) was however, considered separately as the prevailing RH only to simulate OPAC model.
8. Page 8, l.15-16: “as an input” to “as inputs”  
Modified in the revised text.
9. Fig. 8: Top row, Y scale should have been 0-10 km or so, there is not much data seen above that altitude.  
Figure 8 has been modified accordingly.
10. Section 3.3.: key sources of BC aerosols over the stations and nearby should be discussed based on literature (Kumar et al., JGR, 2015)  
Thanks for the suggestion. Authors have addressed the point that diurnal variation in BC was in fact not driven by anthropogenic emissions rather by the changes in the regional meteorology, especially ABL. Authors have included additional discussion on BC sources in the revised text based on Kumar et al. 2015b (Page 11-12, l.29-4).
11. Page 13, l.23: “has” to “have”  
Modified in the revised text.

Title: Aerosol chemistry, transport and climatic implications during extreme biomass burning emissions over Indo-Gangetic Plain  
MS No.: acp-2018-446

Authors sincerely appreciate the careful reviews and suggestions provided by the reviewer and thank the reviewer and the Editor for their time to evaluate the manuscript. Authors have made appropriate changes to the manuscript in response to the comments that have considerably improved the manuscript. In the authors' response, authors have responded point-by-point to comments (reviewer comments in *blue*, authors' responses in *black*), and have included the revisions in the text with and without tracked-changes.

## Authors' Responses to Referee # 2

In this work, the authors carried out a quite comprehensive research on the biomass burning emissions during post-monsoon in South Asia (Indo-Gangetic Plain), involving aerosol composition, transport and radiative forcing. The topic is interesting and important. However, currently the manuscript has some critical problems. The relevant discussion appears just be piled up and superficial. For example, the results of mass concentration, BC, ions, levoglucosan, as well as satellite remote sensing and source areas are already well known in this region. Each subtopic mentioned above actually has already been presented in the literatures. So the authors need to point out what is the new finding from this work. Otherwise, it will undermine the novelty of this study.

Authors highly appreciate such constructive comments and have addressed these issues in the revised manuscript. To authors knowledge, there was no published report available till date on influence of biomass burning on air borne particulate over IGP, measured considering size-segregated particulates ( $PM_{1.1}$ ,  $PM_{1.1-2.1}$ ,  $PM_{>2.1}$ ) and submicron ( $PM_1$ ) particulate chemistry and using satellite data to assess the spatial nature of pollution. Previous reports mainly used  $PM_{2.5}$  or TSP (total aerosols) as matrices to assess emission budget (Rajput et al., 2014), organic mass-to-organic carbon ratio (Rajput and Sarin, 2014), emissions of PAHs (Rajput et al., 2011), organic molecular tracers (Wan et al., 2017) and radiative forcing (Sharma et al., 2017; Alam et al., 2011); while only few have explored remote sensing observations to interpret fire (Vadrevu et al., 2012). Considering completely diverse physicochemical properties of submicron and coarser particulates, our analysis was novel especially in terms of:

1. Integrating satellite & ground-based observations to assess impact over the ground-station and across IGP.
2. First report considering size-segregated aerosols ( $PM_{1.1}$ ,  $PM_{1.1-2.1}$  and  $PM_{>2.1}$ ) with detail aerosol chemistry for  $PM_{1.1}$ .
3. First report on  $PM_{1.1}$  bound PAHs and organics tracers like Levoglucosan during biomass burning emissions.
4. We have also reported spatial and vertical distribution of air pollutants & its short-term variations across IGP.
5. First report on time-series of total and smoke aerosol extinction profile during biomass burning emissions.

These novel aspects of the manuscript have been addressed in introduction (page 3, l.6-27).

Specific comments:

1. Page 5, Line 22-26, here the authors did not mention Ca, K, Na in the analysis, although they are presented in Figure 3 and related discussions. So how did you measure these major elements? For the trace elements, the information of data quality control is also lack. It is well known that the quartz filters have high blank values for some trace elements.

Authors admit there was a mistake and in the revised text Ca, K, Na were added in the methodology (section 2.3.3, page 5, l.25). These metals were also analyzed by AAS along with other trace metals.

Yes, authors agree with reviewer's point that the quartz filters have high blank values for some trace metals. However, their levels were very low in comparison to ambient samples. For metal analysis, the blank filter

papers (unexposed quartz filters) were treated and analyzed similarly like real ambient samples. The measured trace metal concentrations in the blank samples were further deducted from the metal concentration from ambient samples to have metal concentration in ambient air.

Actually, according to the discussion (In section 3.2.2), the contents regarding trace elements is not closely related to the theme of this work (i.e. biomass burning). So I suggest to delete this part.

Authors are thankful for such constructive comments. There are evidences of trace metal emissions from burning of biomass, especially in PM<sub>1</sub>. Likewise, Wang et al. (2015) have concluded biomass combustion as the most prominent source of Fe concentration in submicron particles. For global emission estimation of Fe, Wang et al. (2015) showed combustion as predominant emission source of Fe over Indo-Gangetic plain in comparison to dust. Beside Fe, there are also reports of trace metals emissions particularly K, Cu, S, Zn, Pb from burning of rice-straw (Ryu et al., 2012); organic bound Fe<sup>2+</sup>, Cu<sup>2+</sup>, Ni<sup>2+</sup>, Zn<sup>2+</sup> from hardwood burning (Graham et al., 2011) and Cu, Pb, Ni, As from the burning of biomass fuel (Zhang 2014).

Considering these evidences, authors have included a detail discussion (Page 11, l. 6-23) on submicron (PM<sub>1.1</sub>) and PM<sub>1.1-2.1</sub> bound metals in the manuscript. Briefly, a massive increase in Fe (59-415%) and in K (119-528%) concentration is reported for submicron and fine aerosols during biomass burning period.

2. For the organic compounds, similarly, I can not judge the quality of the analysis in this work. What is the recovery, accuracy or precision of the organic compounds?

Authors are thankful for reviewers' suggestion to improve the QA/QC of analytical procedure. Authors wish to state that we have performed the routine recovery test of organic compounds before the sample analysis and now this has been included in the revised manuscript (Page 6, l.11-14). The recoveries of organic compounds were tested by spiking the known concentration of standard compounds on the pre-combusted quartz filters. They were extracted and analyzed in identical to the real samples. The average recoveries and respective RSD (in parenthesis) of the n-alkanes (28 compounds) ranged from 72-92% (1-12%), phthalates (6 compounds) ranged from 75-88% (2-7%), FAMES ranged from 74-92% (1-9%), PAHs ranged from 73-93% (1-10%) and anhydrosugars (3 compounds) ranged from 75-80% (4-6%, data may be shared if required). To improve the clarity, we have incorporated the recovery of organic compounds and RSD in the revised text (Page 6, l.11-14).

3. Page 12, Line 15-16, reference is needed here. And it's better to give more explanation.

Authors have modified the section 3.3 with additional justifications to the BC sources considering relevant references like Kumar et al., 2015b; Wang et al., 2011; Kumar et al., 2016. Authors have addressed that the diurnal variation in BC concentration was primarily influenced by the changes in the regional meteorology, especially ABL (Page 11-12, l.29-4). In contrast, for daily variation in BC, there was a clear influence of additional anthropogenic emissions like biomass burning during November. This was established with the increase in Delta-C that represent smoke emissions from biomass burning (Wang et al., 2011; Kumar et al., 2016).

4. Line 31-32. Yes, PAHs is important for the study of emissions from biomass/fossil combustion. However, if you can not give proper interpretation of PAHs results, I suggest to delete it.

To our knowledge, this is the first report of submicron particulate bound PAHs during extensive biomass burning period over IGP. There were only few efforts to characterize the PAHs in PM<sub>2.5</sub> and TSP bound aerosols across IGP for biomass burning emissions (like by Chen et al., 2015; Rajput et al., 2011). In revised text authors have strengthen the discussions on PM<sub>1.1</sub> and PM<sub>1.1-2.1</sub> bound PAHs considering all the relevant references which have accounted the biomass burning emissions (Page 13, l.4-11).

5. In this work, many items (organic tracers, major ions) were determined in the laboratories. However, organic carbon and elemental carbon (OC/EC) was not included. Obviously, it is very vital to interpret the results of organic tracers combined with OC/EC, considering the focus of this work is biomass burning.

Authors agree that the consideration of OC/EC would have additionally strengthened the discussions on organic tracers. We wished to include EC/OC measurement, but our quartz samples were limited in terms of particulate exposure. We have used Non-Viable Anderson Cascade Impactor (Tisch, USA) for particulate sampling which gives the deposition of aerosol particles in the form of dots (dia. 1mm or less), scattered on filter disc. For EC/OC analysis, the measurement assumes that aerosol particles are uniformly deposited on filter disc and concentrations are measured in terms of unit area. However, it would have not possible to measure the area of each dot and accurately quantify the EC/OC concentration for cascade samples.

6. Section 3.5, here levoglucosan was introduced in details. Actually it already been presented in section 3.4. (Page 12, Line 33). So some changes are needed for a better logic.

In section 3.4, authors emphasized only on characterizing organic compounds in size-segregated aerosols and levoglucosan concentration was discussed with reference to other available literature.

However, in section 3.5, the emphasis was solely to establish relationship of levoglucosan with other established biomass burning markers, to find out the type of biomass burning and their short-term variations. So, the perspective was different for discussions related to levoglucosan and its isomers in section 3.4 and 3.5.

7. Page 13, Line 23, here you mean the ratio is  $L/(M+G)$ ?

Authors believe that the reviewer wished to indicate the term 'ratio' cited in line 3 of page 14. Yes, the ratio is in between levoglucosan (L) and sum of mannosan (M) and galactosan (G). We have modified the text for clarity (Page 14, l.3).

8. Page 14, Line 8, it is common to see potassium occurs in crustal minerals

Authors acknowledge the reviewers' comment that K commonly occurs in crustal minerals, but this holds generally true for coarser particulates ( $PM_{>2.5}$ ). As per our understanding, the crustal materials are mostly found in coarser particles and  $K^+$  should have considered from crustal origin if we found elevated  $K^+$  in  $PM_{>2.5}$ . In literature (Banerjee et al., 2015; Chen et al. 2017 and references therein),  $K^+$  concentration in finer particles is well reported of biomass burning origin. Even, we evaluated the association in between levoglucosan and  $K^+$  for all three size fractions and found highly significant correlation only in submicron ( $PM_{<1.1}$ ) followed by fine range particles ( $PM_{1.1-2.1}$ ), referring origin of  $K^+$  mainly from biomass burning emissions.

9. Page 16, Line 12. I do not think so. The variations of CO and NO<sub>2</sub> shown in Figure 7b did not reflect the influence of intensive biomass burning.

Authors have modified the argument in page 16, line 14-17 and conclude that increase in CO and NO<sub>2</sub> profile over IGP is the possible consequences of anthropogenic emissions (including industrial, vehicular and biomass burning emissions), not solely due to the biomass burning.

# Aerosol chemistry, transport and climatic implications during extreme biomass burning emissions over Indo-Gangetic Plain

Nandita Singh<sup>1</sup>, Tirthankar Banerjee<sup>1,2</sup>, Made P. Raju<sup>3</sup>, Karine Deboudt<sup>4</sup>, Meytar Sorek-Hamer<sup>5</sup>, Ram S. Singh<sup>2,6</sup> and Rajesh K. Mall<sup>1,2</sup>

<sup>1</sup>Institute of Environment and Sustainable Development, Banaras Hindu University, Varanasi, India

<sup>2</sup>DST-Mahamana Centre of Excellence in Climate Change Research, Banaras Hindu University, Varanasi, India

<sup>3</sup>High Altitude Cloud Physics Laboratory, Indian Institute of Tropical Meteorology, Pune, India

<sup>4</sup>Laboratoire de Physico-Chimie de l'Atmosphère, Université du Littoral Côte d'Opale, Dunkerque, France

<sup>5</sup>NASA Ames Research Center, Moffett Field, CA, USA

<sup>6</sup>Department of Chemical Engineering and Technology, Indian Institute of Technology (BHU), Varanasi, India

Correspondence to: Tirthankar Banerjee (tb.iesd@bhu.ac.in; tirthankaronline@gmail.com)

## Abstract

The large-scale emissions of airborne particulates from burning of agricultural residues particularly over the upper Indo-Gangetic Plain (IGP) have often been associated with frequent formation of haze, adverse health impacts, modification in aerosol climatology and thereby aerosols impact on regional climate. In this study, short-term variations in aerosol climatology during extreme biomass burning emissions over IGP, and thereby to regional climate were investigated. Size-segregated particulate concentration was initially measured and submicron particles (PM<sub>1.1</sub>) were found to dominate particulate mass within the fine mode (PM<sub>2.1</sub>). Particulate bound water-soluble ions were mainly secondary in nature, primarily composed of sulfate and nitrate. There was evidence of gaseous NH<sub>3</sub> dominating neutralization of acidic aerosol species (SO<sub>4</sub><sup>2-</sup>) in submicron particles, in contrast to crustal dominating neutralization in coarser particulates. Diurnal variation in black carbon (BC) mass ratio was primarily influenced by regional meteorology, while gradual increase in BC concentration was consistent with the increase in Delta-C, referring to biogenic emissions. Influence of biomass burning emissions were established using specific organic (levoglucosan), inorganic (K<sup>+</sup> and NH<sub>4</sub><sup>+</sup>) and satellite-based (UV Aerosol Index, UVAI) tracers. Levoglucosan was the most abundant species within submicron particles (649±177 ng m<sup>-3</sup>), with a very high ratio (>50) against other anhydrosugars, indicating exclusive emissions from burning of agriculture residues. Spatio-temporal distribution of aerosol and few trace gases (CO and NO<sub>2</sub>) were evaluated using both space-borne active and passive sensors. A significant increase in columnar aerosol loading (AOD: 0.98) was evident during extreme biomass burning emissions, with presence of absorbing aerosols (UVAI > 1.5) having low aerosol layer height (~1.5 km). A strong intraseasonality in aerosol cross-sectional altitudinal profile was even noted from CALIPSO, referring dominance of smoke and polluted continental aerosols across IGP. Possible transport mechanism of biomass smoke was established using cluster analysis and concentration weighted ~~of~~-air mass back-trajectories. Short-wave aerosol radiative forcing (ARF) was further simulated considering intraseasonality in aerosol properties, which resulted in considerable increase of atmospheric ARF (135 Wm<sup>-2</sup>) and heating rate (4.3 K day<sup>-1</sup>) during extreme biomass burning emissions compared to non-dominating one (56 W m<sup>-2</sup>, 1.8 K day<sup>-1</sup>). Our analysis may be useful to improve understanding of short-term variation in aerosol chemistry over the IGP and to reduce uncertainties in regional aerosol-climate model.~~We therefore conclude that influence of biomass burning emissions on regional aerosol climatology must need to be studied in much finer scale to improve parameterization of aerosol/ climate model across the region.~~

## 1 **1. Introduction**

2 Aerosols are studied systematically in terms of their potential to influence the transfer of  
3 radiant energy and distribution of latent heat, by which it modifies the Earth's weather and climate.  
4 Aerosols are also associated with nutrient recycling and for governing atmospheric chemistry  
5 (Kanakidou et al., 2018). Aerosol interaction with radiation mainly constitutes its radiative forcing of  
6 climate change (Bellouin et al., 2005; Bond et al., 2013) while, it also modifies the climate by means  
7 of cloud formation processes (Seinfeld et al., 2016). The aerosol-radiation interaction necessitates  
8 understanding of spectrally varying aerosol optical properties, which are associated to particle size  
9 distribution, chemical composition, morphology and mixing states. The representation of aerosol  
10 processes in global/-regional climate models varies considerably and thereby, estimates of aerosol-  
11 radiation interaction still consist significant level of uncertainties (Myhre et al., 2013). This necessitates  
12 extensive regional investigation in terms of aerosol composition and properties for improved  
13 parametrization of aerosol schemes in the regional/-global climate model.

14 The Indo-Gangetic plain (IGP) in South Asia is especially unique in terms of aerosols loading  
15 and diversity that varies over the seasons (Singh et al., 2017a,b; Sen et al., 2017; Sayer et al., 2014;  
16 Kumar et al., 2018). The IGP is often projected to be one of the most vulnerable region in terms of  
17 aerosol induced negative health impacts (Apte et al., 2015) and therefore, numerous observational  
18 and modeling studies were made for better characterization of aerosols (Sen et al., 2017; Moorthy et  
19 al., 2008 and references therein). Recently, Singh et al. (2017a) has concluded the presence of spatial  
20 and seasonal variations in aerosol sources over South Asia, with vehicular emissions, followed by  
21 industrial emissions and secondary aerosols contributing most to fine particulates. Additionally,  
22 individual episodes of specific emissions like from biomass burning (Wan et al., 2017; Rajput et al.,  
23 2011, 2014; Rajput and Sarin, 2014) and use of fire crackers (Kumar et al., 2016) also induce sudden  
24 large-scale changes in aerosol properties, and necessitate extensive investigation for better  
25 representation in regional aerosol model. Post-harvest agricultural residue burning, especially over  
26 upper IGP is projected to release 400 Gg of particulate bound organic aerosols (OA) and 40 Gg of black  
27 carbon (BC, Rajput et al., 2014), almost entirely (90 %) from burning of rice husks (Rajput et al., 2011).  
28 The OA mostly constitute the fine particulate mass (20-90 %) and are reported to be hydrophilic in  
29 nature (Rajput and Sarin, 2014) therefore, pose potential to act as CCN molecule, or at most compete  
30 with sulphate particles (Singh et al., 2017b). Nevertheless, presence of such huge amount of OA may  
31 either lead to a reduction in mean evaporation and modify regional precipitation or may reduce cloud  
32 formation processes by inducing additional heat to the system (Riipinen et al., 2011; Sun and Arriya,  
33 2006). The biomass burning aerosols also impact the Earth's surface albedo by depositing on glaciers.  
34 The net radiative forcing of biomass burning aerosols by aerosol-radiation interactions is close to

1 neutral i.e.  $-0.0$  ( $-0.20$  to  $+0.20$ )  $\text{W m}^{-2}$ , having a gradient with negative forcing from OA and positive  
2 forcing from BC (Myhre et al., 2013). Biomass burning aerosols even evolve due to oxidation (Jimenez  
3 et al., 2009; Vakkari et al., 2014), from gas-phase precursors to semi-volatile secondary OA (SOA) and  
4 finally to highly volatile oxidized gases (e.g. CO and CO<sub>2</sub>), thus warrants molecular characterization and  
5 specific understanding both in terms of composition, atmospheric chemistry, transport and radiative  
6 forcing (Singh et al., 2017b).

7 Several investigations were made over IGP to understand the characteristics of biomass  
8 burning aerosols. Few attempts were made solely using ground-based information e.g. aerosol  
9 emission budget (Rajput et al., 2014), organic mass-to-organic carbon ratio (Rajput and Sarin, 2014),  
10 emissions of PAHs (Rajput et al., 2011), organic molecular tracers (Wan et al., 2017; Li et al., 2014) and  
11 radiative forcing (Sharma et al., 2017; Alam et al., 2011); while few have explored remote sensing  
12 observations to interpret fire (Vadrevu et al., 2012) and aerosol plume characteristics (Kaskaoutis et  
13 al., 2014). However, there is a need to integrate both ground and contemporary satellite-based  
14 information so that spatio-temporal characterization of aerosols and its climatic impacts are assessed  
15 more realistically. In the present analysis complementary measurements from both ground and space-  
16 based platforms are therefore combined to trace the vital signatures of extreme biomass burning  
17 emissions, its chemical evolution, transport and aerosol radiative forcing. Initially, chemical  
18 speciations of size-segregated aerosols are made, supported by black carbon dynamics, molecular  
19 tracers of biomass emissions; and further explored in terms of their relevance to regional  
20 meteorology. The spatial extent of aerosol emission and transport was made using Modern-Era  
21 Retrospective Analysis for Research and Applications (MERRA) atmospheric reanalysis data, Global  
22 Data Assimilation System (GDAS) archives and NCEP/ NCAR Reanalysis data. Further, visualization  
23 from 'A-Train' satellite constellation, from both space-borne passive sensors like MODerate resolution  
24 Imaging Spectroradiometer (MODIS), Ozone Monitoring Instrument (OMI) and active sensor like  
25 Cloud-Aerosol Lidar and Infrared Pathfinder Satellite Observation (CALIPSO) are included. Briefly, the  
26 results are explored to highlight three exclusive but inter-related mechanisms, i.e. aerosol chemistry,  
27 regional transport and radiative forcing, and their intra-seasonal variations over middle IGP, which  
28 may well be useful ~~for improving aerosol scheme~~ in regional climate model.

## 29 **2. Experimental methods**

### 30 **2.1 Site description**

31 Ground-based aerosol measurements were made at the institutional premises of Banaras  
32 Hindu University, Varanasi ( $25.26^\circ\text{N}$ ,  $82.98^\circ\text{E}$ ,  $82$  m AMSL). The ground station typically experiences  
33 a humid sub-tropical climate, with no localized effects of oceans or mountains (Fig. 1). The



1 predominating wind profile is north-westerly which are projected to subsidize over a section of middle  
2 IGP, coinciding well with the ground monitoring station, thereby facilitates gradual accumulation of  
3 aerosols (Kumar et al., 2018). Interestingly enough, the region also experiences a significant diurnal  
4 variation in atmospheric boundary layer (ABL) associated with high convective turbulence that usually  
5 redistribute aerosols to a greater height (Kumar et al., 2015a,b, 2017a). Particulates emitted from  
6 crustal sources, road dust re-suspension, vehicular exhausts and biomass/waste burning are often  
7 reported to constitute the regional aerosols (Singh et al., 2017a).

## 8 **2.2 Micro-meteorology, ABL and wind field**

9 The 24 h average meteorological parameters e.g. temperature, relative humidity (RH) and  
10 wind speed (WS) were obtained from wunderground.com and validated with regional weather  
11 monitoring station data. The ABL heights at specific coordinate were retrieved from Global Data  
12 Assimilation System (GDAS) archives hosted at NOAA-Air Resource Laboratory, which provides  
13 simulated meteorological observations at a gridded scale. The 3-hourly ABL data ( $0.5^\circ$ ) were averaged  
14 on daily basis in parallel to period of particulate measurement. The NCEP/NCAR Reanalysis data was  
15 used to measure-analyze the variation of 3-D wind fields at near surface (1000 m) with a horizontal  
16 resolution of  $2.5^\circ \times 2.5^\circ$ . Vector wind composite mean ( $\text{m s}^{-1}$ ) for 925 hPa was plotted for the defined  
17 coordinate ( $6-38^\circ \text{N}$ ,  $50^\circ-105^\circ \text{E}$ ) to understand the synoptic pattern of wind field.

## 18 **2.3 Ground-based measurements**

### 19 **2.3.1 Size-segregated aerosol mass concentration**

20 Size-segregated aerosols were collected on pre-combusted quartz fiber filter using Anderson  
21 eight-stage cascade impactor (Tisch Environmental Inc., USA). Sampling was continued for once in a  
22 week from 1<sup>st</sup> October to 15<sup>th</sup> December 2016, continuously for 72 h (in each week) to get  
23 representative deposition of particulates. The instrument was run with a fix flow rate of 28.3 LPM,  
24 having aerodynamic cut-off diameter of  $<0.43$ ,  $0.65$ ,  $1.1$ ,  $2.1$ ,  $3.3$ ,  $4.7$ ,  $5.8$  and  $>9.0 \mu\text{m}$  (with 50 %  
25 collection efficiency). The individual stages of each sample were then segregated into three groups on  
26 the basis of cut-off diameter (i) coarse mode ( $\text{PM}_{>2.1}$ ) comprising the stages with the aerodynamic  
27 diameter  $>2.1 \mu\text{m}$ ; (ii) fine mode ( $\text{PM}_{1.1-2.1}$ ) for the stages with diameter  $1.1$  to  $2.1 \mu\text{m}$ ; and, (iii)  
28 submicron mode ( $\text{PM}_{<1.1}$ ) for the last two stages with the diameter  $<1.1 \mu\text{m}$ .

### 29 **2.3.2 Black carbon mass concentration**

30 The black carbon (BC) real-time mass concentration was measured using a seven channel  
31 Aethalometer (Model AE-42; Magee Sci. Inc., USA), with a constant flow rate of 3 LPM at 5 minutes  
32 resolution. Aethalometer measures the attenuated beam of light transmitted through aerosol sample

1 on filter tape at seven wavelengths (370, 470, 520, 590, 660, 880 and 950 nm), while attenuation at  
2 880 nm was considered for BC (Bodhaine, 1995). The BC concentration is estimated based on the  
3 concept of linearity between the light attenuation and BC mass deposited on quartz filter. An  
4 absorption efficiency of  $16.6 \text{ m}^2 \text{ g}^{-1}$  (provided by the manufacturer) was used to measure BC after  
5 correction of loading effect. The mechanism for estimation of BC is described in Wang et al. (2011)  
6 and Kumar et al. (2017a). BC measured at two wavelengths e.g. 370 nm (indicating absorption by  
7 wood-smoke particles) and 880 nm (by both fossil fuel and wood burning emissions) were used to  
8 compute Delta-C ( $\text{BC}_{370\text{nm}} - \text{BC}_{880\text{nm}}$ ). Delta-C is reported to symbolize smoke emissions (Wang et al.,  
9 2011; Kumar et al., 2016) and therefore, was used as a tracer for biomass emissions.

### 10 2.3.3 Aerosol chemical constituents

#### 11 *Water-soluble ions*

12 The particulate deposits on filter were extracted with deionized water in an ultrasonic bath  
13 (Microclean-109, Oscar, India) for 30 min, and extracts were further filtered through syringe filters  
14 (pore size  $0.2 \mu\text{m}$ ). The water-soluble ionic constituents (WSIC) were analyzed by ion exchange  
15 chromatograph (ICS 3000, Dionex, USA). For measurement of anions ( $\text{Cl}^-$ ,  $\text{NO}_3^-$ ,  $\text{SO}_4^{2-}$  and  $\text{PO}_4^{3-}$ ), the IC  
16 was equipped with a micro-membrane suppressor (AERS-300, 4 mm; Dionex) with IonPac analytical  
17 column (AS11-HC  $\times$  250-mm) connected with a guard column IonPac (AG11-HC,  $4 \times 50\text{mm}$ ; Dionex).  
18 Cations ( $\text{NH}_4^+$ ,  $\text{Na}^+$ ,  $\text{K}^+$ ,  $\text{Mg}^{2+}$ ,  $\text{Ca}^{2+}$ ) were measured through a suppressor (CERS-300, 4 mm; Dionex)  
19 with an analytical column (IonPac CS12A-HC,  $4 \times 250 \text{ mm}$ ; Dionex) and a guard column (IonPac CG11-  
20 HC,  $4 \times 50 \text{ mm}$ ; Dionex, USA). The background contamination was removed by subtracting the blank  
21 filter value from sample values (Kumar et al., 2017b).

#### 22 *Trace metals*

23 The trace metals were extracted from filter discs as per US EPA Method IO-3.2 (EPA, 1999).  
24 The filters were cut into pieces and digested in acid mixture solution (5.55 %  $\text{HNO}_3$  with 16.67 % HCl)  
25 on a hot plate for 2 h. The extracts were filtered, stored at  $4 \text{ }^\circ\text{C}$  and were analyzed by atomic  
26 absorption spectrophotometer (Avanta Ver 2.01, GBC) for Ca, Na, K, Cu, Mn, Fe, Cd, Cr, Pb, Ni, Co, and  
27 Zn.

#### 28 *Organic compounds*

29 For determining the aerosol organic constituents, the filter composites of each group were  
30 extracted by ultrasonically the filters initially with dichloromethane-hexane mixture (1:1), followed  
31 by dichloromethane-methanol mixture (1:1). Both solvent extracts were combined and concentrated  
32 using vacuum rotary evaporator and nitrogen evaporator to a volume of  $100 \mu\text{L}$  (Hu et al., 2013).

1 The extracts were derivatized by silylation with N, O-bis-(trimethylsilyl)-trifluoroacetamide and 1 %  
2 trimethylchlorosilane prior to analysis. After derivatization, the residue was re-dissolved in hexane  
3 and analyzed by gas chromatography-mass spectrometry (GCMS-QP2010 Ultra, Shimadzu, Japan)  
4 equipped with Rxi-5MS fused silica capillary column having dimension 30 m x 0.25 mm id x 0.25  $\mu\text{m}$   
5 (Restek, Bellefonte, PA, USA). Sample was injected in GCMS at 260°C injector temperature in splitless  
6 mode. The column oven temperature program was started at 50°C with 2 min of the isothermal hold  
7 which further raised up to 120 °C (linear elevation @ 30 °C min<sup>-1</sup>) and 300 °C (linear elevation @ 6 °C  
8 min<sup>-1</sup>) followed by the isothermal hold of 11 min. The electron impact ionization was used to produce  
9 molecular ions at 70 eV with the ion source and interface temperature of 230 °C and 270 °C,  
10 respectively. The molecular ions were scanned for a wide range of m/z from 40 to 650. The target  
11 compounds were identified based on retention time and fragmentation pattern from National  
12 Institute of Standards and Technology (NIST) library and standard solutions of analytes. The average  
13 recoveries (respective RSD) of the n-alkanes (28 compounds) varied from 72-92% (1-12%), 75-88% (2-  
14 7%) for phthalates (6 compounds), 74-92% (1-9%) for FAMES, 73-93% (1-10%) for PAHs and 75-80%  
15 (4-6%) for anhydrosugars (3 compounds).

## 16 **2.4 Satellite-based observations**

### 17 **2.4.1 Aqua/-Terra MODIS data**

18 The aerosol optical depth (AOD) at 550 nm was retrieved daily from MODIS onboard Aqua  
19 satellite in parallel to ground-based aerosol monitoring. The level 2 Collection 6 AOD at 10 km  
20 resolution was retrieved using MODIS merged DT-DB AOD (AOD\_550\_-  
21 Dark\_Target\_Deep\_Blue\_Combined, Levy et al., 2013). The selection of merged DT-DB for retrieving  
22 AOD was based on higher retrieval number and accuracy across the IGP (Mhawish et al., 2017). The  
23 AOD for the ground station was calculated as the average of 5 x 5 pixels, surrounding the monitoring  
24 site. Angstrom exponent (AE,  $\alpha$ ) was retrieved using MODIS C6 level 2 DB AOD and relation between  
25 AOD and AE was used to measure the aerosol loading and the particle size (Kumar et al., 2015a;  
26 Mhawish et al., 2017). Columnar water vapor content (CWV) was retrieved from Aqua MODIS  
27 collection 6 level 2 infrared channel at 1 km spatial resolution. To illustrate the impact of biomass  
28 burning, the fire spots were retrieved over the IGP from Aqua/-Terra MODIS Fire Mapper product  
29 (collection 6, spatial resolution 1x1 km<sup>2</sup>) provided by the Fire Information for Resource Management  
30 System (FIRMS, <https://firms.modaps.eosdis.nasa.gov>). The details about MODIS fire products and its  
31 algorithm may be found elsewhere (Justice et al., 2006).

### 32 **2.4.2 Aura-OMI and MERRA-2 reanalysis data**

1           The OMI onboard AURA satellite has a typical daily global coverage with  $13 \times 24 \text{ km}^2$  spatial  
2 resolution at nadir and measures solar backscatter irradiation in the UV–visible spectrum (264–504  
3 nm; Levelt et al., 2006). Ultraviolet Aerosol Index (UVAI), tropospheric  $\text{NO}_2$ , total columnar ozone  
4 (TCO) and Single scattering albedo (SSA) were retrieved from Aura OMI available at NASA Goddard  
5 Earth Sciences Data and Information Services Centre (GES DISC). Aura OMI UVAI is capable of detecting  
6 aerosol absorption from satellite measured radiances without any prior assumption on aerosol  
7 composition (Torres et al., 2013). It is a qualitative parameter and is widely used to identify the UV  
8 absorbing aerosols (e.g. smoke plumes, soot and mineral dust; Torres et al., 2013; Mhawish et al.,  
9 2018). The UVAI based on OMI near-UV aerosol retrieval algorithm (OMAERUV) was extracted from  
10 Level 2G, version 003 aerosol product containing one day’s Level 2 data set of original pixels ( $13 \times 24$   
11  $\text{km}^2$ ) into  $0.25^\circ \times 0.25^\circ$  grids. The  $\text{NO}_2$  tropospheric column density was retrieved from cloud screened  
12 (cloud fraction  $<30\%$ ) Level 3, version 003, daily  $0.25^\circ \times 0.25^\circ$  gridded OMNO2d product (Krotkov et  
13 al., 2017). To estimate TCO, Level 3e data (OMDOAO3) at a spatial resolution of  $0.25^\circ \times 0.25^\circ$  was used.  
14 SSA at 550 nm was retrieved from OMI level 2G product (OMAERUV) at  $0.25^\circ \times 0.25^\circ$  resolution. The  
15 Carbon Monoxide (CO) surface concentration (in ppbv) was retrieved from Modern-Era Retrospective  
16 Analysis for Research and Applications, version 2 (MERRA-2) atmospheric reanalysis data available at  
17  $0.5^\circ \times 0.625^\circ$  from GES DISC.

### 18 **2.4.3 CALIPSO-CALIOP observations**

19           CALIPSO products were used to examine the vertical distribution of aerosols, altitude of  
20 aerosol layers, clouds, aerosol types and their properties at visible (532nm) and near-IR wavelengths  
21 (1064 nm). The V4.10 CALIOP Level 2 altitude-orbit cross-section profiles obtained from CALIPSO sub-  
22 setting web application (<https://www-calipso.larc.nasa.gov>) was used. The Lidar profiles were  
23 processed for images of vertical feature masks, aerosol subtypes and extinction coefficients (at 532  
24 nm) at 30 m vertical resolution over the selected grid ( $80^\circ$ – $86^\circ\text{N}$  and  $22^\circ$ – $28^\circ\text{E}$ ). The details about data  
25 products, calibration and uncertainty are discussed in Rogers et al. (2011).

### 26 **2.5 Air-mass back trajectory**

27           The NOAA HYSPLIT model (Draxler and Rolph, 2003) was used to simulate particle back  
28 trajectories in a three-dimensional system. The HYSPLIT was run on using the Global Data Assimilation  
29 System data (GDAS,  $0.5^\circ \times 0.5^\circ$ ) available from archive dataset (<http://ready.arl.noaa.gov/gdas1.php>)  
30 to predict 120 h air-mass back trajectories (00:00, 06:00, 12:00 and 18:00 UTC) starting from October  
31 to December 2016. Trajectories for different aerosol loading periods were then overlaid on MODIS  
32 fire map to study the transboundary movement of emissions from biomass burning. The trajectory  
33 analysis was made using GIS-based software TrajStat (Wang et al., 2009). Concentration weighted

1 trajectories (CWT) were also drawn considering columnar aerosol loading to evaluate potential  
2 aerosol source fields and mechanism of aerosol transport. The specificities of the models' parameters  
3 and algorithms are detailed elsewhere (Wang et al., 2009; Kumar et al., 2018).

## 4 **2.6 Aerosol optical properties, radiative forcing and heating rate**

5 Aerosol induced shortwave (0.2–4.0  $\mu\text{m}$ ) direct radiative forcing (ARF) was estimated using  
6 Santa Barbara DISORT Atmospheric Radiative Transfer (SBDART) model (Ricchiazzi et al., 1998). The  
7 SBDART estimates plane-parallel radiative transfer in a clear sky condition for both Earth's top of the  
8 atmosphere (TOA) and at the surface (SUF), while atmospheric forcing (ATM) is calculated as the  
9 difference between them. The standard atmospheric profile is used together with input variables e.g.  
10 AOD, SSA, CWV, TCO and asymmetry parameter (ASP) derived through OPAC model (Optical  
11 Properties of Aerosols and Clouds; Hess et al., 1998). The OPAC provides aerosol optical properties  
12 over a wide range of wavelength and delivers necessary input to SBDART. Mean mass concentrations  
13 of aerosol water soluble (WSIC) and insoluble (dust and organics) components along with BC mass  
14 concentration were converted to particle number densities and introduced to OPAC to derive aerosol  
15 optical properties. ~~The OPAC derived outputs were tuned in respect to measured relative humidity.~~  
16 The AOD and SSA were reconstructed to match modelled and satellite derived values within  $\pm 5\%$   
17 deviation.

18 The weekly mean values of AOD, SSA, ASP, CWV, TCO, visibility and AE were included as ~~an~~  
19 inputs to SBDART. The SBDART includes multiple scattering in a vertically inhomogeneous, non-  
20 isothermal plane-parallel media, and is reported to be efficient in resolving the radiative transfer  
21 equation (Raju et al., 2016). The ARF was calculated using 10 solar zenith angles (0 to 89, with  
22 increment of 10) and was proceed for conditions like 'with aerosols' or 'without aerosols'. The surface  
23 albedo was decided based on visual observation considering a combination of snow, ocean, sand and  
24 vegetation. Overall uncertainty in the estimated ARF was in the range of 10–15 % (Alam et al., 2011).  
25 The ATM-ARF was further used to compute atmospheric heating rate ( $\partial T/\partial t$ ,  $\text{K day}^{-1}$ ), using equation  
26 (1):

$$27 \quad \partial T/\partial t = (g/C_p) * (\Delta F/\Delta P) \quad (1)$$

28 where  $\Delta P$  is the difference in forcing,  $\Delta P$  is the pressure difference between top and bottom boundary  
29 layer,  $C_p$  is specific heat capacity of air at constant pressure and  $g$  is the acceleration due to gravity  
30 (Kumar et al., 2017a).

## 31 **3. Results and discussion**

### 32 **3.1 General characteristics of aerosols**

1           The weekly variation in particulate concentrations in different size fractions are presented in  
2 Fig. 2 with the descriptive statistics included in Table S1. The total aerosol mass concentrations have  
3 high intra-seasonal variations (median: 370; range: 134-734  $\mu\text{g m}^{-3}$ ), mainly influenced by coarse mode  
4 particles ( $\text{PM}_{>2.1}$ ) contributing  $63\pm 15$  % of particulate mass. In contrast, contribution of submicron  
5 ( $\text{PM}_{<1.1}$ :  $27\pm 12$  %) and fine mode particles ( $\text{PM}_{1.1-2.1}$ :  $10\pm 4$  %) to total aerosol loading were relatively  
6 less (<37%). The average ( $\pm 1\sigma$ ) mass concentration of  $\text{PM}_{2.1}$  ( $\text{PM}_{<1.1} + \text{PM}_{1.1-2.1}$ ) and total aerosol loading  
7 was 162 ( $\pm 123$ ) and 390 ( $\pm 199$ )  $\mu\text{g m}^{-3}$ , which were approximately 98 % (against  $\text{PM}_{2.5}$ ) and 92 % higher  
8 compared to annual averages observed over the monitoring station (Murari et al., 2017; Prajapati and  
9 Tripathi, 2008). To our knowledge, till the submission of the manuscript, there were no published  
10 reports on submicron particle over the ground station. Time-series analysis of size-segregated  
11 particulates (Fig. 2) indicate the submicron ( $\text{PM}_{<1.1}$ ) and fine mode particles ( $\text{PM}_{1.1-2.1}$ ) only had a late  
12 rise in mass concentrations, while the coarse mode particulates ( $\text{PM}_{>2.1}$ ) did not show any trend.  
13 However, there was a definite increasing pattern in fine to coarse particle ratio ( $\text{PM}_{2.1}/\text{PM}_{>2.1}$ ; mean:  
14  $0.7\pm 0.5$ ; range: 0.2-1.5), due to a continuous increase of the fine mode from mid-November to the  
15 end of the monitoring. Thus the contribution of fine mode particle to total aerosol loading increased  
16 from mid-November (>40 %), and contributed almost 60 % of particulate mass during the month of  
17 December. The submicron particles also indicate a high median concentration ( $96 \mu\text{g m}^{-3}$ ) compared  
18 to fine mode ( $33 \mu\text{g m}^{-3}$ ), and the particle ratio ( $\text{PM}_{<1.1}/\text{PM}_{1.1-2.1}$ ) remain >1 throughout, only to exceed  
19 values >2.5 from November to December. This clearly indicates the dominance of submicron particles  
20 within fine mode fractions, possibly associated to anthropogenic emissions, and also influenced by  
21 local meteorological conditions e.g. low temperature (mean $\pm$ SD:  $20\pm 3$  °C), calm wind (mean:  $0.6 \text{ m s}^{-1}$ )  
22 and shallow boundary layer height (mean $\pm$ SD:  $379\pm 89$  m).

### 23 **3.2 Aerosol chemical speciations**

#### 24 *3.2.1 Water soluble inorganic species (WSIS)*

25           Temporal variation of WSIS in size-segregated airborne particulates are presented in Fig. 3a.  
26 It indicates the major contribution of WSIS to submicron (21 %) and fine particle mass (21 %) compared  
27 to the coarser one (13 %). The secondary inorganic aerosols ( $\text{SIA} = \text{SO}_4^{2-} + \text{NO}_3^- + \text{NH}_4^+$ ) together  
28 accounted for 17 % of the submicron particle mass, with major contributions from sulfate (9%) and  
29 nitrate (6 %). Similar was the case for fine particulates as SIA contributed to almost 17 % of aerosol  
30 mass with predominate contribution from sulfate (8 %) and nitrate (6 %), and a relatively small  
31 proportion of ammonia (4 %). In contrast, the relative contribution of SIA to coarse particulate was  
32 lower (7 %), also primarily associated to sulfate (5 %) and nitrate compounds (2 %). This indicates the  
33 secondary nature of origin of fine and submicron particles which possibly evolve through gas-phase  
34 photochemical conversion of  $\text{SO}_2$  and  $\text{NO}_2$ , eventually neutralized by crustal species like carbonate

1 salts ( $\text{CaCO}_3$  and  $\text{MgCO}_3$ ) associated with the airborne dust. The time-series of SIA contribution to  
2 particulate mass (Fig. 3a) indicate a dominance (although in different extent) of secondary aerosols in  
3  $\text{PM}_{1.1-2.1}$  and  $\text{PM}_{>2.1}$  only during November.

4 Among the WSIS,  $\text{SO}_4^{2-}$  was invariably the most abundant species within each particulate size  
5 fraction ( $\text{PM}_{<1.1}$ : 39 %,  $\text{PM}_{1.1-2.1}$ : 32 %,  $\text{PM}_{>2.1}$ : 36 %), followed by  $\text{NO}_3^-$  ( $\text{PM}_{<1.1}$ : 27 %,  $\text{PM}_{1.1-2.1}$ : 29 %,  
6  $\text{PM}_{>2.1}$ : 17 %). The  $\text{NO}_3^- / \text{SO}_4^{2-}$  ratio was considered as an indicator of the mobile and stationary source  
7 contribution to nitrogen and sulfur (Tian et al., 2016). An average ratio varying from 0.62 to 1.92 was  
8 noted for all size-segregated particulates testifying dominance of both sources, although in different  
9 time-scales. In later phase, the ionic ratio ( $\text{NO}_3^- / \text{SO}_4^{2-}$ ) enhanced ( $>1$ ) in submicron and fine mode  
10 particles, well identical to the reported haze events over Guangzhou (Tan et al., 2009) and Suzhou,  
11 China (Tian et al., 2016). A very high  $\text{NO}_3^- / \text{SO}_4^{2-}$  ratio ( $3.2 \pm 1.3$ ) was only noted in fine aerosols during  
12 October, mainly due to lower concentration of sulphate. The next two dominant contributors to WSIS  
13 were  $\text{NH}_4^+$  ( $\text{PM}_{<1.1}$ : 14 %,  $\text{PM}_{1.1-2.1}$ : 19 %,  $\text{PM}_{>2.1}$ : 5 %) and  $\text{K}^+$  ( $\text{PM}_{<1.1}$ : 8 %,  $\text{PM}_{1.1-2.1}$ : 5 %,  $\text{PM}_{>2.1}$ : 2 %),  
14 both considered as a molecular tracer for biogenic emission (Banerjee et al., 2015). They constitute  
15 the greater proportion of WSIS in  $\text{PM}_{<1.1}$  and  $\text{PM}_{1.1-2.1}$ , especially from last week of October till the end  
16 of November, signifying elevated contribution of biomass/ agro-residue burning emissions to these  
17 particle sizes. Further, a strong correlation ( $R^2=0.9$ ) between  $\text{NH}_4^+$  and  $\text{SO}_4^{2-}$  and high  $\text{NH}_4^+/\text{SO}_4^{2-}$   
18 equivalent ratio ( $0.9 \pm 0.2$ ) for submicron particulates indicate the abundance of gaseous  $\text{NH}_3$  to  
19 neutralize acidic species ( $\text{SO}_4^{2-}$ ) by forming  $(\text{NH}_4)_2\text{SO}_4$  and/or  $\text{NH}_4\text{HSO}_4$ . The  $\text{NH}_4^+/\text{SO}_4^{2-}$  equivalent ratio  
20 gradually increased from week 5 (mean: 1.2, range: 0.9-1.3), possibly due to abundant emission of  
21  $\text{NH}_4^+$  from biomass emissions. Unlike submicron particles, the low  $\text{NH}_4^+/\text{SO}_4^{2-}$  equivalent ratios ( $<0.7$ ,  
22 mean: 0.4) in coarse mode particles indicate the predominant neutralization by crustal minerals.

23 Unlike the other WSIS,  $\text{Na}^+$  and  $\text{Ca}^{2+}$  were found to contribute maximum in  $\text{PM}_{>2.1}$  ( $\text{Na}^+$ : 2 %;  
24  $\text{Ca}^{2+}$ : 3 %), referring their crustal origin. The relative abundance of  $\text{Cl}^-$  in size-segregated aerosols was  
25 roughly equal for each size fraction, contributing almost in identical to total WSIS in  $\text{PM}_{<1.1}$  (6 %),  $\text{PM}_{1.1-2.1}$   
26  $\text{PM}_{>2.1}$  (5 %) and  $\text{PM}_{>2.1}$  (4 %). The possible origin of  $\text{Cl}^-$  in  $\text{PM}_{>2.1}$  could be the aged sea salt, transported  
27 from Bay of Bengal, but its association with  $\text{PM}_{<1.1}$  was most likely due to biomass burning emissions  
28 (Pavuluri et al., 2011; Murari et al., 2015). The temporal variations of WSIS in all particulate size  
29 fractions were consistent except for  $\text{Mg}^{2+}$  and  $\text{PO}_4^{3-}$  contributing  $<0.2$  % of particulate mass and having  
30 non-biomass specific emission sources. A strong correlation between the anion and cation equivalents  
31 within all the size groups (0.7-0.9) indicate that the most ions were from the filter samples. The total  
32 ion equivalent ratio (anions to cation) refer a cationic imbalance ( $\text{PM}_{<1.1}$ : 1.2,  $\text{PM}_{1.1-2.1}$ : 0.8 and  $\text{PM}_{>2.1}$ :  
33 0.6) with excess cations in fine and coarse mode particles, possibly due to unmeasured components  
34 like carbonates and bicarbonates.

### 1 3.2.2 Trace metals

2 Total metallic contribution to particulate mass was found maximum in  $PM_{1.1-2.1}$  (24 %),  
3 followed by  $PM_{>2.1}$  (11 %) and least in  $PM_{<1.1}$  (7 %, Fig. 3b). The most abundant elements were Na, Ca,  
4 K and Zn for all size fractions, contributing 90-98 % of total identified metals, while the remaining  
5 fractions were primarily constituted by Fe (1-10 %). Within the detectable level of metals, Ca and Na  
6 share 88 % of metal concentrations in  $PM_{<1.1}$  and 7% of submicron particulate mass, without having  
7 any specific temporal trend. However, Ca, Na were found high in  $PM_{1.1-2.1}$  (Ca: 10 %; Na: 7 %), referring  
8 their origin from resuspension of crustal materials and road dust.

9 There are few evidences of trace metal emissions from burning of biomass. Wang et al. (2015)  
10 have concluded biomass combustion as the most prominent source of Fe concentration in submicron  
11 particles. For this analysis, although Fe was measured maximum in  $PM_{>2.1}$ , the relative increase in Fe  
12 concentration in submicron ( $PM_{1.1}$ : 59 %) and fine aerosols ( $PM_{1.1-2.1}$ : 415 %) during week 6 to week 9  
13 possibly indicate the added contribution of biomass burning emissions. Beside Fe, there are also  
14 reports of trace metals emissions particularly K, Cu, S, Zn, Pb from burning of rice-straw (Ryu et al.,  
15 2012); organic bound  $Fe^{2+}$ ,  $Cu^{2+}$ ,  $Ni^{2+}$ ,  $Zn^{2+}$  from hardwood burning (Chang-Graham et al., 2011) and  
16 Cu, Pb, Ni, As from the burning of biomass fuel (Zhang 2014). In our case, massive increase in K ( $PM_{1.1}$ :  
17 528 %;  $PM_{1.1-2.1}$ : 119 %) was also noted between week 6 and week 9. This contrasted with coarse  
18 particle bound Fe and K which are primarily of crustal origin (Banerjee et al., 2015), and recorded only  
19 15 % (Fe) and 83 % (K) increase in concentration within week 6 to 9. Zinc was found considerably high  
20 in  $PM_{>2.1}$  (3 %) and relatively small proportion in  $PM_{1.1-2.1}$  (2 %). The major sources of atmospheric Zn  
21 are burning of residual oil, refuse and garbage (Gonzalez et al., 2016) which possibly leads to higher  
22 mass fractions in coarser particulates. Here, a relatively high Zn concentration was noted in later phase  
23 of monitoring irrespective of particulate size coincide with the winter specific burning of waste/  
24 refuse over the region (Kumar et al., 2017b). The relative contribution of rest of the trace metals (e.g.  
25 Mn, Pb, Cd, Ni, Cu, Cr and Co) to particulate mass were insignificant (<0.05 %), without having any  
26 specific temporal pattern.

### 27 3.3 Characteristics of BC mass loading

28 Daily means of BC concentration and Delta-C ( $BC_{370} - BC_{880}$ ) are plotted in Fig. 4 with some  
29 data gaps. The 24 h average BC concentration varied from 2.0-15.4  $\mu g m^{-3}$  with a seasonal mean ( $\pm 1\sigma$ )  
30 of 8.3 ( $\pm 2.9$ )  $\mu g m^{-3}$ . The season specific BC average was 80 % higher in comparison to annual mean  
31 (4.6  $\mu g m^{-3}$ ; Kumar et al., 2017a), while there were also reports of winter-specific very high BC  
32 concentration (22  $\mu g m^{-3}$ ; Murari et al., 2016) that usually persist over the region. A distinct diurnal  
33 profile with high BC concentration during nighttime ( $>9 \mu g m^{-3}$ ; 11:00-7:00 h) and low daytime-BC



1 concentration ( $<6 \mu\text{g m}^{-3}$ , 11:00-17:00 h) was also noted. Gradual rise in BC mass loading concentration  
2 from 17:00 h ~~well coincide with the traffic rush hours. However, the rest of BC diurnal profile is could~~  
3 ~~be mainly mainly~~ attributed to the ~~variation regional meteorology in boundary layer height~~, which  
4 ~~otherwise is considered reported as theas the most most important influential~~ factor in regulating BC  
5 ~~concentrations after the source itself compared to the anthropogenic sources~~ (Kumar et al.,  
6 ~~20162015b~~, 2017a). Regional meteorology, particularly boundary layer height and transport are two  
7 fundamental processes that influence the diurnal BC variation, mainly by means of regulating  
8 horizontal and vertical transport (Kumar et al., 2015b). Therefore, the diurnal variation in BC  
9 concentration were the consequence of change in boundary layer height with occasional inflow of  
10 emissions from large-scale burning of agriculture residues/ biomass/ waste and from vehicular  
11 emissions.

12 The BC timeseries shows an enhanced BC concentration from the end of October (week 4) till  
13 the November end (week 9). Such increase in BC concentration was however, possibly due to  
14 increased source strength as there was no significant variation in meteorological variables (like ABL)  
15 within this timeframe (Table S1). ~~Therefore, we hypothesize that the variation in BC source strength~~  
16 ~~might have well influenced the BC concentration.~~ To understand the variation in BC sources, 24 h  
17 average Delta-C concentration (mean $\pm$ SD:  $2.3\pm 1.0 \mu\text{g m}^{-3}$ ) is also included in Fig. 4, which ~~also~~ refers  
18 ~~the emission of smoke a temporal shift in BC sources particles (Wang et al., 2011; Kumar et al., 2016).~~  
19 Except few exceptions, high Delta-C ( $>2.3 \mu\text{g m}^{-3}$ ) was observed particularly in the month of November  
20 (80 % of days) compared to October (23%) and December (46 %), referring added contribution of  
21 biomass burning emissions.

### 22 **3.4 Composition of organic aerosols**

23 Size-segregated particle-bound organic aerosols (OA) were analysed for 22 *n*-alkanes ( $\text{C}_{13}$ - $\text{C}_{34}$ ),  
24 3 anhydrosugars (levoglucosan, mannosan and galactosan), 4 PAHs and 10 *n*-alkanoic acids ( $\text{C}_{12}$ - $\text{C}_{26}$ )  
25 (Fig. 5). Considerable variation in the concentration and size distributions of these OA were  
26 noted. Contributions of OA to size-segregated particulates were relatively less because of partial  
27 characterization through GC-MS. Among the identified species, *n*-alkanes were invariably the highest  
28 within  $\text{PM}_{<1.1}$  (mean $\pm$ SD:  $484\pm 103 \text{ ng m}^{-3}$ ) compared to fine ( $267\pm 43 \text{ ng m}^{-3}$ ) and coarse mode aerosols  
29 ( $308\pm 93 \text{ ng m}^{-3}$ ). The molecular distribution of *n*-alkanes homologues in all three size fractions showed  
30 a slight dominance of odd-numbered *n*-alkanes. The CPI (Carbon Preference Index) remain close to  
31 unity (CPI range: 1.2-2.1; mean $\pm$ SD:  $1.5\pm 0.5$ ), indicating dominance of anthropogenic emissions like  
32 combustion of fossil fuels and biomass burning. The higher molecular weight homologues ( $>\text{C}_{25}$ )  
33 concentration were found highest in  $\text{PM}_{<1.1}$  with an oscillating pattern, having odd molecules  
34 concentration higher than the adjacent even molecules (Fig. 5b). In contrast the low molecular weight

1 homologues ( $<C_{25}$ ) showed no such specific pattern of odd/even dominance. The sources of higher  
2 homologues ( $C_{27}$ ,  $C_{29}$  and  $C_{31}$ ) are probably the surface deposited plant litter for coarse mode and  
3 biomass burning for fine mode aerosols, while low molecular weight homologues ( $<C_{25}$ ) primarily  
4 originate from the fossil fuel combustion (Kang et al., 2016). Saturated fatty acids were found to  
5 constitute a larger fraction of solvent extractable organics within coarse mode ( $439\pm 38$  ng  $m^{-3}$ )  
6 and submicron particles ( $357\pm 162$  ng  $m^{-3}$ ) in comparison to fine mode ( $171\pm 57$  ng  $m^{-3}$ ). For all three  
7 size fractions, total low molecular weight fatty acids ( $\leq C_{20}$ ) concentration was found higher than the  
8 high molecular weight fatty acids ( $\geq C_{20}$ ), indicating the anthropogenic emissions like vehicular,  
9 residential biomass burning and energy practices. Presence of high concentration of  $C_{12}$ , and  $C_{15}$  refer  
10 the dominance of cooking oil combustion. The high concentration of  $C_{22}$  further suggests the influence  
11 of biomass burning which potentially emit both, high and low fatty acids (Mochida et al., 2007). The  
12 fatty acid amide was found in trace amount which could possibly be derived from fatty acid and  
13 ammonia during burning process. Presence of PAHs was also measured for size-segregated  
14 particulates and was found highest in submicron particulates ( $7.0$  ng  $m^{-3}$ ) compared to  $PM_{1.1-2.1}$  ( $3.6$  ng  
15  $m^{-3}$ ) and  $PM_{>2.1}$  ( $3.1$  ng  $m^{-3}$ ). ere PAHs are mainly produced due to incomplete combustion of fuels like  
16 fossil fuels and biomass at relatively high temperature (Singh et al., 2017b; Chen et al., 2015). There  
17 was no previous report of submicron particulate bound PAHs during biomass burning emissions over  
18 IGP, except for  $PM_{2.5}$  bound PAHs in Patiala ( $27-40$  ng  $m^{-3}$ ; Rajput et al., 2011, 2014), Agra ( $9$  ng  $m^{-3}$ ;  
19 Villalobos et al., 2015), Kanpur ( $3$  ng  $m^{-3}$ ; Villalobos et al., 2015) and total aerosol bound PAHs in  
20 Kathmandu ( $320$  ng  $m^{-3}$ , Chen et al., 2015).

21 Levoglucosan was found to be the most abundant anhydrosugar in submicron particles with  
22 an average ( $\pm 1\sigma$ ) of  $649$  ( $\pm 177$ ) ng  $m^{-3}$ . In contrast, concentration in fine ( $229\pm 87$  ng  $m^{-3}$ ) and coarse  
23 particles ( $162\pm 68$  ng  $m^{-3}$ ) were relatively low, referring the influence of biomass burning emissions for  
24 submicron particles. Levoglucosan concentration measured in this study are well comparable to other  
25 reported observations, especially with the cases that have accounted the influence of biomass burning  
26 emissions e.g. New Delhi ( $1978$  ng  $m^{-3}$ , Li et al., 2014), Mt. Tai, China ( $391$  ng  $m^{-3}$ , Fu et al., 2008), Gent,  
27 Belgium ( $477$  ng  $m^{-3}$ , Zdrahal et al., 2002), Lumbini, Nepal ( $734$  ng  $m^{-3}$ , Wan et al., 2017) and Beijing,  
28 China ( $590$  ng  $m^{-3}$ , Cheng et al., 2013). Beside levoglucosan, relative concentration of other  
29 anhydrosugars (mannosan and galactosan) in all size-segregated aerosols were negligible ( $<70$  ng  $m^{-3}$ ,  
30 not shown).

### 31 **3.5 Signature of biomass burning emissions**

32 Biomass primarily consists of different bio polymers (e.g. cellulose, hemicellulose, lignin,  
33 suberin, sporopollenin and chitin) with small proportion of lipids and terpenoids. During thermal  
34 combustion, such biomass emits different types of organic molecules, some of which ~~has~~ have the

1 potential to be considered as signature molecule based on their long residence time and chemical  
2 stability (Banerjee et al., 2015). The major combustion product of cellulose and hemicellulose includes  
3 anhydrosugars like levoglucosan (1,6-anhydro- $\beta$ -D-glucopyranose,  $C_6H_{10}O_5$ ) and its two isomers  
4 (mannosan and galactosan). Among these, levoglucosan is a robust and widely used tracer for biomass  
5 burning emissions, both globally (Simoneit et al., 1999; Schkolnik et al., 2005; Cheng et al., 2013), and  
6 over IGP (Li et al., 2014; Banerjee et al., 2015; Wan et al., 2017). In our case, levoglucosan was  
7 abundant in submicron particles with a peak during November (week 6 to 9, Fig. 6). The rise in  
8 concentration was universal in each particulate size fractions, but typically in submicron ( $837 \pm 83$  ng  
9  $m^{-3}$ ) and fine particulates ( $311 \pm 47$  ng  $m^{-3}$ ), having 54-70 % rise against rest of the monitoring period.  
10 This could correspond to a short-term variation in emissions source strength which possibly well  
11 influenced the aerosol property. A ratio between levoglucosan with rest of the anhydrosugars  
12 (mannosan and galactosan)-was also considered to indicate the dominating type of biomass burning,  
13 with a ratio  $<10$  specific for softwood combustion, and  $>10$  for burning of hardwood and crop residues  
14 (Cheng et al., 2013). Even a ratio  $>40$  was reported from physical experiments using rice straw, wheat  
15 straw and maize stalks (Engling et al., 2009). Although, the presence of mannosan and galactosan was  
16 not frequent in our case, but an overall ratio  $>50$  refers the exclusive dominance of agriculture residue  
17 burning across the IGP.

18 The possibility of considering  $K^+$  and  $NH_4^+$  as biomass burning tracers were investigated in  
19 terms of their association with levoglucosan for submicron and fine particulates. In general, the  
20 temporal trend of levoglucosan coincided well with both  $K^+$  and  $NH_4^+$ , and all these tracers registered  
21 a gradual rise in concentration during November. Highly significant correlation ( $R^2$ ) between  
22 levoglucosan and  $K^+$  ( $PM_{1.1}$ : 0.80,  $PM_{1.1-2.1}$ : 0.76;  $p < 0.01$ ), and levoglucosan and  $NH_4^+$  ( $PM_{1.1}$ : 0.95,  $PM_{1.1-2.1}$ :  
23 0.60;  $p < 0.01$ ) were noted at 99 % confidence interval. That definitely indicates that levoglucosan,  
24  $K^+$  and  $NH_4^+$  have similar biogenic sources over IGP which predominately contribute to the aerosol  
25 loading, especially in  $PM_{1.1}$  and  $PM_{1.1-2.1}$ . The relation between levoglucosan with  $K^+$  and  $NH_4^+$  further  
26 appeared to be non-linear, with an exponential fit for submicron ( $R^2$ : 0.84, 0.94) and for fine  
27 particulates ( $R^2$ : 0.83, 0.65). Non-linear correlations between levoglucosan and  $K^+$  are also reported at  
28 Amazon (Schkolnik et al., 2005) and in Beijing (Cheng et al., 2013) during extreme biomass burning  
29 emissions. There was also evidence that  $NH_4^+$  was better associated with levoglucosan compared to  
30  $K^+$ , referring the presence of additional  $K^+$  sources across the region (like fireworks, Kumar et al., 2016).  
31 However, in absence of aerosol organic carbon content, contribution of biomass burning to aerosol  
32 mass was not computed.

33 Besides using conventional biomass burning tracers, we also evaluated the association of  
34 submicron and fine particulate bound levoglucosan with weekly averages of Delta-C and UVAI (Fig. 6).

1 Both Delta-C and UVAI are the measures of identifying the relative dominance of absorbing aerosols.  
2 In all scenarios, significant correlation ( $R^2$ ) was noted between levoglucosan with Delta-C (0.65,  
3  $p < 0.01$ ) and UVAI (0.66,  $p < 0.01$ ). In addition to the ground-based aerosol measurement, dynamic  
4 profile of trace gases concentration, especially for those that behave as aerosol precursors, are  
5 assessed from Real-time Air Quality Data inventory of Central Pollution Control Board  
6 (<https://app.cpcbccr.com/ccr>). The hourly average concentrations of individual trace gases were  
7 initially checked for data quality and outliers, and further averaged to 24 h. No such universal trend in  
8 concentration of all the trace gases was evident, except an overall increasing trend for NO, NO<sub>2</sub>, NO<sub>x</sub>,  
9 and CO, while SO<sub>2</sub> remained stable and there was a negative trend for O<sub>3</sub>. The most striking feature  
10 was to have an increase in concentration particularly during November, although of different  
11 magnitude. This was also evident in the variation of particulate bound biomass tracers, which inspire  
12 us to consider two different aerosol loading scenarios *viz.* scenario 1 for biomass burning dominating  
13 period (week 6 to 9, BDP) and scenario 2 for biomass burning less dominant period (week 1-5 and  
14 week 10-11, BLDP). Such classification was intended to recognize if there was any variation in aerosol  
15 source fields over IGP and in aerosol-induced radiative forcing.

### 16 **3.6 Spatio-temporal nature of aerosol columnar properties**

17 Spatio-temporal variations in aerosol columnar properties and trace gases are plotted in Fig.  
18 7a, including the daily variations at the ground station (Fig. 7b). Instead of considering the columnar  
19 properties for the entire season, spatial plots are generated for two different scenarios like BDP and  
20 BLDP.

21 The spatial pattern in aerosol columnar properties was typical having a very high aerosol  
22 loading exclusively over IGP (area weighted AOD mean $\pm$ SD: 0.55 $\pm$ 0.21) in comparison to the rest of  
23 South Asia (0.31 $\pm$ 0.21). However, there was no such temporal variation particularly over IGP as both  
24 BDP<sub>AOD</sub> (0.56 $\pm$ 0.23) and BLDP<sub>AOD</sub> (0.53 $\pm$ 0.23) was almost similar. The BDP<sub>AOD</sub> was slightly higher (12 %  
25 to that of reported decadal average (0.50 $\pm$ 0.25, Kumar et al. 2018), and was comparable to the season  
26 specific average over IGP (0.55 $\pm$ 0.20; Kumar et al., 2018). It should be noted that area weighted AOD  
27 average includes all the pixels retrieved across the region, some of which may not represent the  
28 biomass emissions. This leads us to further retrieve and compare AOD particularly over the ground  
29 station. In this case, the mean AOD was significantly high during post-monsoon (0.81 $\pm$ 0.39), 44 %  
30 higher for BDP<sub>AOD</sub> (0.98 $\pm$ 0.42) in respect of BLDP<sub>AOD</sub> (0.68 $\pm$ 0.32). Even, the BDP<sub>AOD</sub> was 46 % higher  
31 compared to decadal average for the station (0.67 $\pm$ 0.28; Kumar et al., 2018). Figure 7a also includes a  
32 comparison of relative dominance of aerosol types in terms of AE, and in both conditions fine particles  
33 (AE; BDP: 1.5, BLDP: 1.7) were found to dominate with a season specific mean ( $\pm 1\sigma$ ) of 1.6 ( $\pm 0.2$ ).

1 Following the evidence of persisting high AOD and high AE indicating dominance of fine  
2 particulates of anthropogenic origin, the nature of aerosols in terms of absorbing and/or scattering  
3 was distinguished using OMI UVAI. UVAI has been widely used to detect dust (Badarinath et al., 2010),  
4 biomass burning aerosols (Torres et al., 2013; Kaskaoutis et al., 2014) and soot particles (Kumar et al.,  
5 2016), and has also been used in combination with CALIPSO to detect height of aerosol layer (Guan et  
6 al., 2010). In our experiment, the daily UVAI varied from (-) 0.34 to (+) 2.24 with a seasonal mean ( $\pm 1\sigma$ )  
7 of 0.99 ( $\pm 0.49$ ) over IGP, which is considerably higher than the seasonal mean for entire South Asia  
8 ( $0.47 \pm 0.46$ ). Interestingly, negative UVAI was only evident during early October (week 1) signifying  
9 presence of non-absorbing aerosols (like sulphate), while UV absorbing aerosols such as smoke and/  
10 or mineral dust was mainly evident during rest of the season. During BDP, the high UVAI values ( $>1.5$ )  
11 were mainly found to concentrate over the upper to middle IGP with 72 % of observations remain  
12  $>1.0$ . This clearly indicates the larger abundance of fresh UV-absorbing particles, and is similar to the  
13 reported UVAI ( $<2.0$ ) over the Himalayas during peak burning season (Kumar et al., 2011; Vadrevu et  
14 al., 2012). There was also considerable difference between the periodical mean UVAI for BDP  
15 ( $1.47 \pm 0.64$ ) and BLDP ( $0.75 \pm 0.58$ ) over the ground station. Further, following Guan et al. (2010) to use  
16 UVAI as a proxy to compute aerosol height, we found a low average height of aerosol layer ( $\sim 1.5$  km),  
17 possibly due to low-altitude injection of plumes from burning of agricultural residues.

18 Apart from aerosols, spatial variation of few trace gases (e.g. CO and NO<sub>2</sub>), directly emitted  
19 from biomass burning are also estimated. The MERRA-2 reanalysis surface CO profile was consistent  
20 with the observed UVAI, with high CO surface concentration over IGP (mean $\pm$ SD:  $156 \pm 62$  ppbv) in  
21 contrast to South Asia ( $114 \pm 52$  ppbv). Similar was the case for tropospheric NO<sub>2</sub> column density as  
22 Aura OMI observation show higher NO<sub>2</sub> concentration across IGP ( $2.4 \pm 1.1 \times 10^{15}$  mol.cm<sup>-2</sup>) compared  
23 to South Asia ( $1.5 \pm 1.0 \times 10^{15}$  mol.cm<sup>-2</sup>). Dominance of CO and NO<sub>2</sub> across IGP clearly reflect the  
24 influence of ~~There was definite spatial signature of the influence of biomass anthropogenic~~  
25 ~~emissions from industries, vehicles and biomass burning on these trace gases, while their~~  
26 ~~abundance may also have influenced by other anthropogenic sources (like industry and vehicular~~  
27 ~~emissions).~~ Likewise, higher surface NO<sub>2</sub> concentrations ( $> 5 \times 10^{15}$  mol cm<sup>-2</sup>) were particularly evident  
28 over urban/-industrial hotspots like Punjab and Delhi, over industrial sectors in the Chhattisgarh and  
29 in lower IGP (particularly over Dhaka). ~~However, episode-specific spatial~~ Temporal variations in mean  
30 CO (143 to 169 ppbv) and NO<sub>2</sub> concentrations ( $2.3$  to  $2.5 \times 10^{15}$  mol cm<sup>-2</sup>) were not so severe both  
31 across IGP and over ground station (CO: 140-142 ppbv; NO<sub>2</sub>:  $2.3$ - $2.5 \times 10^{15}$  mol cm<sup>-2</sup>). The possible  
32 explanation for such minimum episode-specific variation may be the short residence time of NO<sub>2</sub> and  
33 CO, as NO<sub>2</sub> rapidly photo-dissociate by reaction with OH radical, while CO gradually oxidized to form  
34 CO<sub>2</sub>. Overall, spatio-temporal nature of aerosols and trace gases were consistent with the observed

1 trend at the ground station and were prudent for establishing the influence of biomass emissions over  
2 the region.

### 3 **3.7 Vertical distribution of aerosols**

4 Vertically resolved aerosol subtypes from spaceborne lidar for selected overpasses across IGP  
5 are plotted in Fig. 8a, with corresponding extinction coefficient of aerosol type (Fig. 8b). The CALIPSO-  
6 CALIOP profile clearly indicates a temporal change in aerosol type, without any considerable change  
7 in the height of aerosol layer. During initial days (in October), dominance of polluted dust (dust mixed  
8 with biomass burning smoke) were noted across IGP, with occasional prevalence of smoke (biomass  
9 burning aerosols), clean continental (clean background aerosol) and dust aerosols. However, the  
10 contribution of polluted dust to total aerosol extinction was higher compared to the rest of aerosol  
11 type. The height of aerosol layer was relatively low (<2 km) corresponding to a low plume injection  
12 height and thereby, pose limited potential for dispersion. The aerosol vertical profile however,  
13 modified from the end of October due to biomass burning emissions, with dominance of smoke  
14 particles, mainly persisting at low altitude (<1.5 km). The height of smoke layer was consistent to that  
15 of OMI UVAI projected aerosol height. Smoke particles were found to associate with polluted dust,  
16 clean continental and polluted continental, with overlapping profiles. Overall, smoke was the most  
17 frequent aerosol type with high aerosol extinction coefficient ( $1-2.5 \text{ Km}^{-1}$  at 532 nm), and the altitude  
18 of largest occurrence frequency of smoke remain below  $\sim 1.5$  km. The low injection height of smoke  
19 plumes from biomass burning may serve as a key input for aerosol transport modeling over IGP, as it  
20 critically regulates the distance and direction of the particle dispersion (Guan et al., 2010; Banerjee et  
21 al., 2011).

22 The daily variation in total aerosol extinction and aerosol extinction only by smoke particles  
23 were also included in Fig. 8c. Total aerosol extinction indicates a corresponding increase during  
24 biomass burning which peaks particularly in November, with low smoke injection height. Clear  
25 evidence of gradual increase in smoke particle aerosol extinction was also noted. A single evidence of  
26 high smoke extinction ( $>1 \text{ Km}^{-1}$ ) at a greater height ( $\sim 3.4$  km) was noted on November 11, which may  
27 be associated to particles travelling from a larger distance. Overall, the CALIOP aerosol profiles were  
28 in accordance to the ground observations and OMI UVAI, referring exclusive dominance of high UV-  
29 absorbing aerosols across the plain during intense biomass burning.

### 30 **3.8 Potential aerosols sources and transport**

31 Active fire counts from the Terra and Aqua MODIS fires and thermal anomalies (with  $\geq 70\%$   
32 confidence) clearly indicate that fire spots were predominately over the upper IGP, mainly  
33 concentrated over the Indian state of Punjab, Haryana and western Uttar Pradesh, and in Punjab state

1 of Pakistan (Fig. 9). However, there was a temporal shift in the total number of fire counts (Fig. 9,  
2 within the marked region) from biomass burning dominating period (BDP: 5272) to less dominating  
3 period (BLDP: 4466). Even, the Fire Radiative Power (FRP) i.e. rate of energy released in unit time  
4 indicates a relative change in amount and strength of biomass burning emissions, mainly during BDP  
5 (138,366 MW) in comparison to BLDP (112,168 MW). The total FRP was higher during BDP mainly due  
6 to higher number of fire counts and fire strength, as the rate of release of thermal radiation is related  
7 to the amount of biomass burnt and smoke being released (Schroeder et al., 2010). The MODIS fire  
8 spots (with brightness temperature), specially subset over IGP were plotted against five days air-mass  
9 back trajectories, simulated and integrated at three vertical heights (100m, 300m and 500m) over the  
10 ground station. Vertical heights were selected based on the average planetary boundary layer height  
11 ( $402\pm 81$  m) for the monitoring period. The air-mass back trajectories indicate the upper IGP as the  
12 sole source of aerosols during BDP, which was otherwise influenced by both continental and marine  
13 air-masses during non-dominating period. The air-mass back trajectories during BDP overlap precisely  
14 on the fire spots that corresponds to higher brightness temperature, referring greater relevance to  
15 FRP. The air masses for individual episode were further subject to cluster and CWT analysis considering  
16 columnar aerosol load, and result was consistent with our prior observations. High CWT ( $>0.8$ ) during  
17 BDP was clearly attributed to the regional pollution, mainly originated from the upper IGP. In contrast,  
18 relatively low CWT was noted during BLDP, originating both from upper IGP ( $CWT < 0.8$ ), western dry  
19 region ( $CWT < 0.6$ ) and few from oceanic environment ( $CWT < 0.4$ ). This leads us to conclude with  
20 confidence that there was a strong temporal gradient in post-monsoon specific biomass burning  
21 emission over the upper IGP, which greatly influence the regional aerosol climatology and thereby,  
22 influence the aerosol-induced health effects and regional climate.

### 23 **3.9 Aerosol radiative forcing and atmospheric heating**

24 Daily satellite retrieved AOD, TCO, CWV, SSA, ground-based BC mass concentration, aerosol  
25 water soluble and insoluble fractions were used as an input to OPAC model to simulate aerosol  
26 radiative forcing (ARF at 0.2-4.0  $\mu\text{m}$ ). Within the period, TCO varied between 237 to 277 DU without  
27 any difference between BDP ( $257\pm 10$  DU) and BLDP ( $256\pm 12$  DU). The SSA (at 550nm), designates the  
28 fraction of scattered light over the total light extinction, was lower during BDP ( $0.86\pm 0.05$ ) compared  
29 to BLDP ( $0.98\pm 0.04$ ), suggesting abundance of strong absorbing aerosols especially during BDP. The  
30 CWV also fluctuates considerably (range: 0.28-3.92 cm) with overall season specific mean ( $\pm\sigma$ ) of 2.0  
31 ( $\pm 0.7$ ) cm.

32 The direct ARF and heating rate were estimated under clear-sky conditions with SBDART  
33 model using OPAC output. The composite ARF was calculated for individual episodes at surface (SRF),  
34 top of the atmosphere (TOA) and atmosphere (ATM) (Fig. 10). Overall, the ARF at TOA and SRF were

1 negative, indicating the aerosol cooling effect at surface and at top-of-the-atmosphere. There was a  
2 slight temporal change in TOA radiative forcing (BDP: -28; BLDP: -23 W m<sup>-2</sup>) compared to the  
3 considerable intra-seasonal variation in SRF forcing (BDP: -163; BLDP: -79 W m<sup>-2</sup>). The variation in SRF  
4 forcing was mainly induced by the surface BC (mean; BDP, BLDP: 9, 7 μg m<sup>-3</sup>), aerosol mass  
5 concentration (501, 327 μg m<sup>-3</sup>) and WSIC fractions, particularly in SO<sub>4</sub><sup>2-</sup> (38, 15 μg m<sup>-3</sup>), NO<sub>3</sub><sup>-</sup> (19, 12  
6 μg m<sup>-3</sup>) and NH<sub>4</sub><sup>+</sup> (11, 4 μg m<sup>-3</sup>). Since the ATM forcing is the balance of attenuation of radiation at TOA  
7 and SRF, the resultant atmospheric forcing was found very high, especially during biomass burning  
8 dominated period (BDP: 135 W m<sup>-2</sup>), compared to non-dominating one (BLDP: 56 W m<sup>-2</sup>). Overall, there  
9 was a clear indication of intraseasonal variation in aerosol radiative forcing, which needs to consider  
10 in parametrization of aerosol schemes for regional climate model. Similarly, the corresponding heat  
11 rate was substantially high during BDP (4.3 K day<sup>-1</sup>), possibly influenced by more absorbing aerosols,  
12 compared to BLDP (1.8 K day<sup>-1</sup>). The computed ARF during post-monsoon was comparable to other  
13 urban sites in Indo-Gangetic Plain that are reported to be influenced by biomass burning e.g. Delhi  
14 (44-131 W m<sup>-2</sup>, Bisht et al., 2015), Patiala (57-63 W m<sup>-2</sup>, Sharma et al. 2017), Kanpur (30-43 W m<sup>-2</sup>,  
15 Kaskaoutis et al., 2013) and over Karachi (35-84 W m<sup>-2</sup>, Alam et al., 2011). However, none of the earlier  
16 reports noted the intraseasonality in ARF by means of change in driving factors which, appeared to be  
17 significant, and necessitate proper addressing in regional model simulation. Intraseasonality in ARF  
18 was earlier reported over Varanasi during winter (ARF: 31-47 W m<sup>-2</sup>, Kumar et al., 2017b), while the  
19 change in forcing was not as drastic as evident during post-monsoon. Therefore, it is extremely likely  
20 that intraseasonality in aerosol properties significantly influence the aerosol-climate-health  
21 interactions over IGP and therefore, must need to be taken in to account for uncertainty analysis in  
22 the regional aerosol/-climate model.

#### 23 **4. Conclusions**

24 The influence of biomass burning emissions on aerosol properties, transport and radiative  
25 forcing was evaluated over Indo-Gangetic plain, South Asia. Very high concentration of total and fine  
26 mode aerosol (PM<sub>2.5</sub>) were observed during post-monsoon, with significant increase in fine to coarse  
27 particle ratio (>1) particularly from November. Submicron particles dominate the aerosol fine mode,  
28 with PM<sub>1.1</sub> to PM<sub>1.1-2.1</sub> ratio frequently exceeding 2.5. The WSIS was found to constitute greater  
29 proportion of submicron and fine particle mass compared to the coarser one. The WSIS was mainly of  
30 secondary nature, with major contribution from sulfate and nitrate ions. A strong correlation between  
31 NH<sub>4</sub><sup>+</sup> and SO<sub>4</sub><sup>2-</sup>, and high NH<sub>4</sub><sup>+</sup>/SO<sub>4</sub><sup>2-</sup> equivalent ratio in submicron particulates indicate the abundance  
32 of gaseous NH<sub>3</sub> to neutralize acidic species (SO<sub>4</sub><sup>2-</sup>). This contrasted with coarse mode particles where  
33 low NH<sub>4</sub><sup>+</sup>/SO<sub>4</sub><sup>2-</sup> equivalent ratio refers the predominant neutralization by crustal minerals. The NO<sub>3</sub><sup>-</sup> to  
34 SO<sub>4</sub><sup>2-</sup> ratio for submicron and fine mode particles also increased (>1) during extreme biomass



1 emissions, as expected considering other reported observations of haze events over Asia. A rise in  
2 black carbon with corresponding increase in Delta-C refer to the added contribution of biomass  
3 burning emissions. The influence of emissions was further quantified using specific organic  
4 (Levoglucosan), inorganic ( $K^+$  and  $NH_4^+$ ) and satellite (UVAI) tracers. Levoglucosan was the most  
5 abundant species in submicron particles, with a very high ratio ( $>50$ ) against other anhydrosugars  
6 denoting exclusive emissions from burning of agriculture residues. The temporal variation in  
7 levoglucosan was consistent with inorganic tracers ( $K^+$  and  $NH_4^+$ ), with a sharp rise during November,  
8 and a strong correlation between these three indicates their biogenic sources. The association  
9 between levoglucosan and  $K^+$  or  $NH_4^+$  was non-linear, with an exponential fit for submicron and fine  
10 particulates. The spatio-temporal distribution of aerosols was evaluated in terms of area weighted  
11 mean both over IGP and over the selected transect across ground station. During biomass burning  
12 dominated period, a considerable increase in columnar aerosol loading was highlighted (AOD: 0.98),  
13 consisting absorbing aerosols (UVAI  $> 1.5$ ) with a corresponding low plume height ( $\sim 1.5$  km).  
14 Moreover, the variation of few trace gases associated with biomass emissions ( $CO$  and  $NO_2$ ) were  
15 consistent with AOD, allowing a definite spatial signature of emissions sources and transport across  
16 IGP. The CALIPSO-CALIOP cross-sectional altitudinal profiles clearly illustrate the intraseasonality in  
17 aerosol types that were dominated by smoke and polluted continental aerosols during biomass  
18 emissions, which otherwise associate to clean continental, polluted dust and dust aerosols. The  
19 possible pathway for regional transport of aerosols from upper IGP to the ground station was noted  
20 using cluster analysis and concentration weighted air mass back-trajectories. Finally, aerosol optical  
21 and micro-physical properties were used in combination to simulate direct aerosol radiative forcing  
22 (ARF) and atmospheric heating. There was evidence of strong intraseasonality in ARF with very high  
23 atmospheric forcing ( $135 \text{ Wm}^{-2}$ ) and heating rate ( $4.3 \text{ Kday}^{-1}$ ) during biomass burning dominated  
24 period compared to non-dominating one ( $56 \text{ Wm}^{-2}$ ,  $1.8 \text{ Kday}^{-1}$ ).

25         Considering that the duration of these biomass burning emissions represents several weeks  
26 per year, there annual impact on ARF and by consequent on the regional climate is not negligible. We  
27 therefore, conclude with reasonable level of confidence that intraseasonality in aerosol properties  
28 must be seriously considered in the regional aerosol-climate model, for improve assessment and  
29 forecasting of aerosol-climate-health interactions across IGP.

### 30 **Data availability**

31         MODIS data are available at Level 1 Atmosphere Archive & Distribution System (LAADS) at  
32 <https://ladsweb.nascom.nasa.gov>. Aura-OMI and MERRA 2 reanalysis data are available at Mirador-  
33 NASA Goddard Earth Sciences Data and Information Center (GES DISC)  
34 (<https://mirador.gsfc.nasa.gov>). CALIPSO data are available at NASA Atmospheric Science Data Center

1 (<https://eosweb.larc.nasa.gov>). Planetary Boundary Layer height and air mass back-trajectories are  
2 retrieved from Global Data Assimilation System (GDAS) archives hosted at NOAA-Air Resource  
3 Laboratory (<https://ready.arl.noaa.gov>). Modis Fire products are obtained from Fire Information for  
4 Resource Management System (FIRMS) (<https://firms.modaps.eosdis.nasa.gov>). Trace gases data at  
5 ground station are available at Real time Air Quality Data inventory of Central Pollution Control Board  
6 (<https://app.cpcbccr.com/ccr>).

7

8 **Team List.** Nandita Singh (NS), Tirthankar Banerjee (TB), Made P. Raju (MPR), Karine Deboudt (KD),  
9 Meytar Sorek-Hamer (MSH), Ram S. Singh (RSS) and Rajesh K. Mall (RKM).

#### 10 **Author Contributions**

11 N.S. and T.B. designed the experiment while N.S., M.P.R. and T.B. carried out the experiment and  
12 analyzed the data. N.S., M.P.R., K.D., T.B., R.S.S., R.K.M. and M.S.H. interpreted the observation and  
13 N.S., T.B. and K.D. drafted the manuscript.

14 **Competing interests.** The authors declare that they have no conflict of interest.

#### 15 **Acknowledgements**

16 The research is supported by Science and Engineering Research Board (SERB), Department of Science  
17 and Technology (DST), New Delhi (SR/FTP/ES-52/2014). T.B. acknowledges the financial support from  
18 University Grants Commission (UGC) under UGC-ISF bilateral project (6-11/2018 IC), R.S.S.  
19 acknowledges the Indian Space Research Organization (ISRO), Thiruvananthapuram under ARFI (Code:  
20 P-32-13) and R.K.M. acknowledges DST under Prime Ministers National Action Plan on Climate Change  
21 project (DST/CCP/CoE/80/2017-G). N.S. acknowledges the financial support under DST Women  
22 Scientist scheme (SR/WOS-A/EA-1012/2015) and M.S.H. acknowledges the NASA Post-Doctoral  
23 Fellowship, administered by USRA. Authors duly acknowledge the guidance and cooperation provided  
24 by Dean and Director, IESD-BHU.

#### 25 **References**

26 Alam, K., Trautmann, T., and Blaschke, T.: Aerosol optical properties and radiative forcing over mega-city  
27 Karachi, *Atmos. Res.*, 101, 773-782, <https://doi.org/10.1016/j.atmosres.2011.05.007>, 2011.

28 Apte, J.S., Marshall, J.D., Cohen, A.J., and Brauer, M.: Addressing global mortality from ambient PM<sub>2.5</sub>, *Environ.*  
29 *Sci. Technol.*, 49, 8057-8066, <https://pubs.acs.org/doi/10.1021/acs.est.5b01236>, 2015.

30 Badarinath, K.V.S., Sharma, A.R., Kaskaoutis, D.G., Kharol, S.K., and Kambezidis, H.D.: Solar dimming over the  
31 tropical urban region of Hyderabad, India: Effect of increased cloudiness and increased anthropogenic  
32 aerosols. *J. Geophys. Res.-Atmos.*, 115, D21208, <https://doi.org/10.1029/2009JD013694>, 2010.

33 Banerjee, T., Murari, V., Kumar, M., and Raju, M.P.: Source apportionment of airborne particulates through  
34 receptor modeling: Indian scenario. *Atmos. Res.*, 164, 167-187,  
35 <https://doi.org/10.1016/j.atmosres.2015.04.017>, 2015.

- 1 Banerjee, T., Barman, S.C., Srivastava, R.K.: Application of air pollution dispersion modeling for source-  
2 contribution assessment and model performance evaluation at Integrated Industrial Estate-Pantnagar.  
3 *Environ Pol.*, 159, 865-875, <https://doi.org/10.1016/j.envpol.2010.12.026>, 2011.
- 4 Bellouin, N., Boucher, O., Haywood, J., and Reddy, M.S.: Global estimate of aerosol direct radiative forcing from  
5 satellite measurements, *Nature*, 438, 1138–1141, <https://doi.org/10.1038/nature04348>, 2005.
- 6 Bisht, D.S., Dumka, U.C., Kaskaoutis, D.G., Pipal, A.S., Srivastava, A.K., Soni, V.K., Attri, S.D., Sateesh, M., and  
7 Tiwari, S.: Carbonaceous aerosols and pollutants over Delhi urban environment: temporal evolution,  
8 source apportionment and radiative forcing, *Sci. Total Environ.*, 521, 431-445,  
9 <https://doi.org/10.1016/j.scitotenv.2015.03.083>, 2015.
- 10 Bodhaine, B.A.: Aerosol absorption measurements at Barrow, Mauna Loa and the south pole, *J. Geophys. Res.-*  
11 *Atmos.*, 100, 8967-8975, <https://doi.org/10.1029/95JD00513>, 1995.
- 12 Bond, T.C., Doherty, S.J., Fahey, D.W., Forster, P.M., Berntsen, T., DeAngelo, B.J., Flanner, M.G., Ghan, S.,  
13 Kärcher, B., Koch, D., and Kinne, S.: Bounding the role of black carbon in the climate system: A scientific  
14 assessment, *J. Geophys. Res.-Atmos.*, 118, 5380-5552, <https://doi.org/10.1002/jgrd.50171>, 2013.
- 15 Chang-Graham, A.L., Profeta, L.T., Johnson, T.J., Yokelson, R.J., Laskin, A. and Laskin, J.: Case study of water-  
16 soluble metal containing organic constituents of biomass burning aerosol, *Environ. Sci. Technol.*, 45,1257-  
17 1263, <https://doi.org/10.1021/es103010j>, 2011.
- 18 Cheng, Y., Engling, G., He, K.B., Duan, F.K., Ma, Y.L., Du, Z.Y., Liu, J.M., Zheng, M., and Weber, R.J.: Biomass  
19 burning contribution to Beijing aerosol, *Atmos. Chem. Phys.*, 13(15), 7765-7781,  
20 <https://doi.org/10.5194/acp-13-7765-2013>, 2013.
- 21 [Chen, P., Kang, S., Li, C., Rupakheti, M., Yan, F., Li, Q., Ji, Z., Zhang, Q., Luo, W., and Sillanpää, M.: Characteristics](#)  
22 [and sources of polycyclic aromatic hydrocarbons in atmospheric aerosols in the Kathmandu Valley, Nepal,](#)  
23 [Sci. Total Environ. 538, 86-92, https://doi.org/10.1016/j.scitotenv.2015.08.006, 2015.](#)
- 24 Draxler, R.R., and Rolph, G.D., 2003. HYSPLIT (HYbrid single-particle Lagrangian integrated trajectory) model  
25 access via NOAA ARL READY. NOAA Air Resources Laboratory, Silver Spring, MD. Dostupno na:  
26 <http://ready.arl.noaa.gov/HYSPLIT.php> (06. 06. 2010.).
- 27 Engling, G., Lee, J.J., Tsai, Y.W., Lung, S.C.C., Chou, C.C.K., and Chan, C.Y.: Size-resolved anhydrosugar  
28 composition in smoke aerosol from controlled field burning of rice straw, *Aerosol Sci. Technol.*, 43, 662-  
29 672, <https://doi.org/10.1080/02786820902825113>, 2009.
- 30 Fu, P., Kawamura, K., Okuzawa, K., Aggarwal, S.G., Wang, G., Kanaya, Y., and Wang, Z.: Organic molecular  
31 compositions and temporal variations of summertime mountain aerosols over Mt. Tai, North China  
32 Plain, *J. Geophys. Res.-Atmos.*, 113, D19107, <https://doi.org/10.1029/2008JD009900>, 2008.
- 33 Gonzalez, R.O., Strekopytov, S., Amato, F., Querol, X., Reche, C., and Weiss, D.: New insights from zinc and copper  
34 isotopic compositions into the sources of atmospheric particulate matter from two major European  
35 cities, *Environ. Sci. Technol.*, 50, 9816-9824, <https://pubs.acs.org/doi/10.1021/acs.est.6b00863>, 2016.
- 36 Guan, H., Esswein, R., Lopez, J., Bergstrom, R., Warnock, A., Follette-Cook, M., Fromm, M., and Iraci, L.T.: A multi-  
37 decadal history of biomass burning plume heights identified using aerosol index measurements, *Atmos.*  
38 *Chem. Phys.*, 10, 6461-6469, <https://doi.org/10.5194/acp-10-6461-2010>, 2010.
- 39 Hess, M., Koepke, P., and Schult, I.: Optical properties of aerosols and clouds: The software package OPAC, *Bull.*  
40 *Am. Meteorol. Soc.*, 79, 831-844, <https://doi.org/10.1175/1520->  
41 [0477\(1998\)079<0831:OPOAAC>2.0.CO;2](https://doi.org/10.1175/1520-0477(1998)079<0831:OPOAAC>2.0.CO;2), 1998.
- 42 Hu, Q.H., Xie, Z.Q., Wang, X.M., Kang, H., and Zhang, P.: Levoglucosan indicates high levels of biomass burning  
43 aerosols over oceans from the Arctic to Antarctic, *Sci. Rep.*, 3, 3119, <https://doi.org/10.1038/srep03119>,  
44 2013.

- 1 Jimenez, J.L., Canagaratna, M.R., Donahue, N.M., Prevot, A.S.H., Zhang, Q., Kroll, J.H., DeCarlo, P.F., Allan, J.D.,  
2 Coe, H., Ng, N.L., and Aiken, A.C.: Evolution of organic aerosols in the atmosphere, *Science*, 326, 1525-  
3 1529, <http://doi.org/10.1126/science.1180353>, 2009.
- 4 Justice, C., Giglio, L., Boschetti, L., Roy, D., Csiszar, I., Morisette, J., and Kaufman, Y.: MODIS Fire Products  
5 Algorithm Technical Background Document. MODIS Science Team, 2006.
- 6 Kanakidou, M., Myriokefalitakis, S., and Tsigaridis, K.: Aerosols in atmospheric chemistry and biogeochemical  
7 cycles of nutrients. *Environ. Res. Lett.*, in press, <https://doi.org/10.1088/1748-9326/aabcbd>, 2018.
- 8 Kaskaoutis, D.G., Kumar, S., Sharma, D., Singh, R.P., Kharol, S.K., Sharma, M., Singh, A.K., Singh, S., Singh, A., and  
9 Singh, D.: Effects of crop residue burning on aerosol properties, plume characteristics, and long-range  
10 transport over northern India, *J. Geophys. Res.-Atmos.*, 119, 5424-5444,  
11 <https://doi.org/10.1002/2013JD021357>, 2014.
- 12 Kaskaoutis, D.G., Sinha, P.R., Vinoj, V., Kosmopoulos, P.G., Tripathi, S.N., Misra, A., Sharma, M., and Singh, R.P.:  
13 Aerosol properties and radiative forcing over Kanpur during severe aerosol loading conditions, *Atmos.*  
14 *Environ.*, 79, 7-19, <https://doi.org/10.1016/j.atmosenv.2013.06.020>, 2013.
- 15 Krotkov, N.A., Lamsal, L.N., Celarier, E.A., Swartz, W.H., Marchenko, S.V., Bucsela, E.J., Chan, K.L., Wenig, M., and  
16 Zara, M.: The version 3 OMI NO<sub>2</sub> standard product, *Atmospheric Meas. Tech.*, 10, 3133-3149,  
17 <https://doi.org/10.5194/amt-10-3133-2017>, 2017.
- 18 Kumar, M., Tiwari, S., Murari, V., Singh, A.K., and Banerjee, T.: Wintertime characteristics of aerosols at middle  
19 Indo-Gangetic Plain: Impacts of regional meteorology and longrange transport, *Atmos. Environ.*, 104,  
20 162-175, <https://doi.org/10.1016/j.atmosenv.2015.01.014>, 2015a.
- 21 [Kumar, R., M.C. Barth, G.G. Pfister, V.S. Nair, S.D. Ghude, and N. Ojha.: What controls the seasonal cycle of black](#)  
22 [carbon aerosols in India?, \*J. Geophys. Res. Atmos.\*, 120, 7788–7812, doi:10.1002/2015JD023298, 2015b.](#)
- 23 Kumar, M., Parmar, K.S., Kumar, D.B., Mhawish, A., Broday, D.M., Mall, R.K., and Banerjee, T.: Long-term aerosol  
24 climatology over Indo-Gangetic Plain: Trend, prediction and potential source fields, *Atmos. Environ.*, 180,  
25 37-50, <https://doi.org/10.1016/j.atmosenv.2018.02.027>, 2018.
- 26 Kumar, M., Raju, M.P., Singh, R.S., and Banerjee, T.: Impact of drought and normal monsoon scenarios on aerosol  
27 induced radiative forcing and atmospheric heating in Varanasi over middle Indo-Gangetic Plain, *J. Aerosol*  
28 *Sci.*, 113, 95-107, <https://doi.org/10.1016/j.jaerosci.2017.07.016>, 2017a.
- 29 Kumar, M., Raju, M.P., Singh, R.K., Singh, A.K., Singh, R.S., and Banerjee, T.: Wintertime characteristics of aerosols  
30 over middle Indo-Gangetic Plain: Vertical profile, transport and radiative forcing, *Atmos. Res.*, 183, 268-  
31 282, <https://doi.org/10.1016/j.atmosres.2016.09.012>, 2017b.
- 32 Kumar, M., Singh, R.K., Murari, V., Singh, A.K., Singh, R.S., and Banerjee, T.: Fireworks induced particle pollution:  
33 a spatio-temporal analysis, *Atmos. Res.*, 180, 78-91, <https://doi.org/10.1016/j.atmosres.2016.05.014>,  
34 2016.
- 35 Kumar, R., Naja, M., Satheesh, S.K., Ojha, N., Joshi, H., Sarangi, T., Pant, P., Dumka, U.C., Hegde, P., and  
36 Venkataramani, S.: Influences of the springtime northern Indian biomass burning over the central  
37 Himalayas, *J. Geophys. Res.-Atmos.*, 116, D19302, <https://doi.org/10.1029/2010JD015509>, 2011.
- 38 Kang, M., Fu, P., Aggarwal, S.G., Kumar, S., Zhao, Y., Sun, Y., and Wang, Z.: Size distributions of n-alkanes, fatty  
39 acids and fatty alcohols in springtime aerosols from New Delhi, India, *Environ. Pollut.*, 219, 957-  
40 966, <https://doi.org/10.1016/j.envpol.2016.09.077>, 2016.
- 41 Levelt, P.F., van den Oord, G.H., Dobber, M.R., Malkki, A., Visser, H., de Vries, J., Stammes, P., Lundell, J.O., and  
42 Saari, H.: The ozone monitoring instrument, *IEEE Trans. Geosci. Remote Sens.*, 44, 1093-1101,  
43 <http://doi.org/10.1109/TGRS.2006.872333>, 2006.

- 1 Levy, R.C., Mattoo, S., Munchak, L.A., Remer, L.A., Sayer, A.M., Patadia, F., and Hsu, N.C.: The Collection 6 MODIS  
2 aerosol products over land and ocean, *Atmospheric Meas. Tech.*, 6, 2989-3034,  
3 <https://doi.org/10.5194/amt-6-2989-2013>, 2013.
- 4 Li, J., Wang, G., Aggarwal, S.G., Huang, Y., Ren, Y., Zhou, B., Singh, K., Gupta, P.K., Cao, J., and Zhang, R.:  
5 Comparison of abundances, compositions and sources of elements, inorganic ions and organic  
6 compounds in atmospheric aerosols from Xi'an and New Delhi, two megacities in China and India, *Sci.*  
7 *Total Environ.*, 476, 485-495, <https://doi.org/10.1016/j.scitotenv.2014.01.011>, 2014.
- 8 Mochida, M., Umemoto, N., Kawamura, K., Lim, H.J., and Turpin, B.J.: Bimodal size distributions of various  
9 organic acids and fatty acids in the marine atmosphere: Influence of anthropogenic aerosols, Asian dusts,  
10 and sea spray off the coast of East Asia, *J. Geophys. Res.-Atmos.*, 112,  
11 D15209, <https://doi.org/10.1029/2006JD007773>, 2007.
- 12 Mhawish, A., Banerjee, T., Broday, D.M., Misra, A., and Tripathi, S.N.: Evaluation of MODIS Collection 6 aerosol  
13 retrieval algorithms over Indo-Gangetic Plain: Implications of aerosols types and mass loading, *Remote*  
14 *Sens. Environ.*, 201, 297-313, <https://doi.org/10.1016/j.rse.2017.09.016>, 2017.
- 15 Mhawish, A., Kumar, M., Mishra, A.K., Srivastava, P.K., and Banerjee, T.: Remote sensing of aerosols from space:  
16 retrieval of properties and applications, In *Remote Sensing of Aerosols, Clouds, and Precipitation*, 45-83,  
17 <https://doi.org/10.1016/B978-0-12-810437-8.00003-7>, 2018.
- 18 Moorthy, K.K., Satheesh, S.K., Babu, S.S., and Dutt, C.B.S.: Integrated Campaign for Aerosols, gases and Radiation  
19 Budget (ICARB): An overview, *J. Earth Syst. Sci.*, 117, 243–262, [https://doi.org/10.1007/s12040-008-](https://doi.org/10.1007/s12040-008-0029-7)  
20 [0029-7](https://doi.org/10.1007/s12040-008-0029-7), 2008.
- 21 Murari, V., Kumar, M., Barman, S.C., and Banerjee, T.: Temporal variability of MODIS aerosol optical depth and  
22 chemical characterization of airborne particulates in Varanasi, India, *Environ. Sci. Pollut. Res.*, 22, 1329-  
23 1343, <https://doi.org/10.1007/s11356-014-3418-2>, 2015.
- 24 Murari, V., Kumar, M., Mhawish, A., Barman, S.C., and Banerjee, T.: Airborne particulate in Varanasi over middle  
25 Indo-Gangetic Plain: variation in particulate types and meteorological influences, *Environ. Monit.*  
26 *Assess.*, 189, 157, <https://doi.org/10.1007/s10661-017-5859-9>, 2017.
- 27 Murari, V., Kumar, M., Singh, N., Singh, R.S., and Banerjee, T.: Particulate morphology and elemental  
28 characteristics: variability at middle Indo-Gangetic Plain, *J. Atmos. Chem.*, 73, 165-179,  
29 <https://doi.org/10.1007/s10874-015-9321-5>, 2016.
- 30 Myhre, G., Samset, B.H., Schulz, M., Balkanski, Y., Bauer, S., Berntsen, T.K., Bian, H., Bellouin, N., Chin, M., Diehl,  
31 T., and Easter, R.C.: Radiative forcing of the direct aerosol effect from AeroCom Phase II  
32 simulations, *Atmos. Chem. Phys.*, 13, 1853-1877, <https://doi.org/10.5194/acp-13-1853-2013>, 2013.
- 33 Pavuluri, C.M., Kawamura, K., Aggarwal, S.G., and Swaminathan, T.: Characteristics, seasonality and sources of  
34 carbonaceous and ionic components in the tropical aerosols from Indian region, *Atmos. Chem. Phys.*, 11,  
35 8215-8230, <https://doi.org/10.5194/acp-11-8215-2011>, 2011.
- 36 Prajapati, S.K., and Tripathi, B.D.: Seasonal variation of leaf dust accumulation and pigment content in plant  
37 species exposed to urban particulates pollution, *J. Environ. Qual.*, 37, 865-870,  
38 <https://doi.org/10.2134/jeq2006.0511>, 2008.
- 39 Rajput, P., and Sarin, M.M.: Polar and non-polar organic aerosols from large-scale agricultural-waste burning  
40 emissions in Northern India: implications to organic mass-to-organic carbon ratio, *Chemosphere*, 103, 74-  
41 79, <https://doi.org/10.1016/j.chemosphere.2013.11.028>, 2014.
- 42 Rajput, P., Sarin, M. M., Sharma, D., and Singh, D.: Characteristics and emission budget of carbonaceous species  
43 from post-harvest agricultural-waste burning in source region of the Indo-Gangetic Plain, *Tellus B*, 66,  
44 21026, <https://doi.org/10.3402/tellusb.v66.21026>, 2014

- 1 Rajput, P., Sarin, M.M., Rengarajan, R., and Singh, D.: Atmospheric polycyclic aromatic hydrocarbons (PAHs) from  
2 post-harvest biomass burning emissions in the Indo-Gangetic Plain: isomer ratios and temporal  
3 trends, *Atmos. Environ.*, 45, 6732-6740, <https://doi.org/10.1016/j.atmosenv.2011.08.018>, 2011.
- 4 Raju, M.P., Safai, P.D., Vijayakumar, K., Devara, P.C.S., Naidu, C.V., Rao, P.S.P., and Pandithurai, G.: Atmospheric  
5 abundances of black carbon aerosols and their radiative impact over an urban and a rural site in SW  
6 India, *Atmos. Environ.*, 125, 429-436, <https://doi.org/10.1016/j.atmosenv.2015.09.023>, 2016.
- 7 Ricchiazzi, P., Yang, S., Gautier, C., and Sowle, D.: SBDART: A research and teaching software tool for plane-  
8 parallel radiative transfer in the Earth's atmosphere, *Bull. Am. Meteorol. Soc.*, 79, 2101-2114,  
9 [https://doi.org/10.1175/1520-0477\(1998\)079<2101:SARATS>2.0.CO;2](https://doi.org/10.1175/1520-0477(1998)079<2101:SARATS>2.0.CO;2), 1998.
- 10 Riipinen, I., Pierce, J.R., Yli-Juuti, T., Nieminen, T., Hakkinen, S., Ehn, M., Junninen, H., Lehtipalo, K., Petaja, T.,  
11 Slowik, J., and Chang, R.: Organic condensation: a vital link connecting aerosol formation to cloud  
12 condensation nuclei (CCN) concentrations, *Atmos. Chem. Phys.*, 11, 3865-3878,  
13 <https://doi.org/10.5194/acp-11-3865-2011>, 2011.
- 14 Rogers, R.R., Hostetler, C.A., Hair, J.W., Ferrare, R.A., Liu, Z., Obland, M.D., Harper, D.B., Cook, A.L., Powell, K.A.,  
15 Vaughan, M.A., and Winker, D.M.: Assessment of the CALIPSO Lidar 532 nm attenuated backscatter  
16 calibration using the NASA LaRC airborne High Spectral Resolution Lidar, *Atmos. Chem. Phys.*, 11, 1295-  
17 1311, <https://doi.org/10.5194/acp-11-1295-2011>, 2011.
- 18 Ryu, S.Y., Kim, J.E., Zhuanshi, H., Kim, Y.J. and Kang, G.U.: Chemical composition of post-harvest biomass burning  
19 aerosols in Gwangju, Korea, *J. Air Waste Manag. Assoc.*, 54, 1124-  
20 1137, <https://doi.org/10.1080/10473289.2004.10471018>, 2004.
- 21 Sayer, A.M., Munchak, L.A., Hsu, N.C., Levy, R.C., Bettenhausen, C., and Jeong, M.J.: MODIS Collection 6 aerosol  
22 products: Comparison between Aqua's e-Deep Blue, Dark Target, and "merged" data sets, and usage  
23 recommendations, *J. Geophys. Res.-Atmos.*, 119, 13,965–13,989,  
24 <https://doi.org/10.1002/2014JD022453>, 2014.
- 25 Schkolnik, G., Falkovich, A.H., Rudich, Y., Maenhaut, W., and Artaxo, P.: New analytical method for the  
26 determination of levoglucosan, polyhydroxy compounds, and 2-methylerythritol and its application to  
27 smoke and rainwater samples, *Environ. Sci. Technol.*, 39, 2744-2752, <http://doi.org/10.1021/es048363c>,  
28 2005.
- 29 Schroeder, W., Csiszar, I., Giglio, L., and Schmidt, C.C.: On the use of fire radiative power, area, and temperature  
30 estimates to characterize biomass burning via moderate to coarse spatial resolution remote sensing data  
31 in the Brazilian Amazon, *J. Geophys. Res.-Atmos.*, 115, D21121, <https://doi.org/10.1029/2009JD013769>,  
32 2010.
- 33 Seinfeld, J.H., Bretherton, C., Carslaw, K.S., Coe, H., DeMott, P.J., Dunlea, E.J., Feingold, G., Ghan, S., Guenther,  
34 A.B., Kahn, R., and Kraucunas, I.: Improving our fundamental understanding of the role of aerosol– cloud  
35 interactions in the climate system, *Proc. Natl. Acad. Sci.*, 113, 5781-5790,  
36 <https://doi.org/10.1073/pnas.1514043113>, 2016.
- 37 Sen, A., Abdelmaksoud, A.S., Ahammed, Y.N., Banerjee, T., Bhat, M.A., Chatterjee, A., Choudhuri, A.K., Das, T.,  
38 Dhir, A., Dhyani, P.P., and Gadi, R.: Variations in particulate matter over Indo-Gangetic Plains and Indo-  
39 Himalayan Range during four field campaigns in winter monsoon and summer monsoon: role of pollution  
40 pathways, *Atmos. Environ.*, 154, 200-224, <https://doi.org/10.1016/j.atmosenv.2016.12.054>, 2017.
- 41 Sharma, D., Srivastava, A.K., Ram, K., Singh, A., and Singh, D.: Temporal variability in aerosol characteristics and  
42 its radiative properties over Patiala, northwestern part of India: Impact of agricultural biomass burning  
43 emissions, *Environ. Pollut.*, 231, 1030-1041, <https://doi.org/10.1016/j.envpol.2017.08.052>, 2017.

- 1 Simoneit, B.R., Schauer, J.J., Nolte, C.G., Oros, D.R., Elias, V.O., Fraser, M.P., Rogge, W.F., and Cass, G.R.:  
2 Levoglucosan, a tracer for cellulose in biomass burning and atmospheric particles, *Atmos. Environ.*, 33,  
3 173-182, [https://doi.org/10.1016/S1352-2310\(98\)00145-9](https://doi.org/10.1016/S1352-2310(98)00145-9), 1999.
- 4 Singh, N., Murari, V., Kumar, M., Barman, S.C., and Banerjee, T.: Fine particulates over South Asia: review and  
5 meta-analysis of PM<sub>2.5</sub> source apportionment through receptor model, *Environ. Pollut.*, 223, 121-136,  
6 <https://doi.org/10.1016/j.envpol.2016.12.071>, 2017a.
- 7 Singh, N., Mhawish, A., Deboudt, K., Singh, R.S., and Banerjee, T.: Organic aerosols over Indo-Gangetic Plain:  
8 Sources, distributions and climatic implications, *Atmos. Environ.*, 157, 59-74,  
9 <https://doi.org/10.1016/j.atmosenv.2017.03.008>, 2017b.
- 10 Sun, J., and Ariya, P.A.: Atmospheric organic and bio-aerosols as cloud condensation nuclei (CCN): A review,  
11 *Atmos. Environ.* 40, 795–820, <https://doi.org/10.1016/j.atmosenv.2005.05.052>, 2006.
- 12 Tan, J.H., Duan, J.C., Chen, D.H., Wang, X.H., Guo, S.J., Bi, X.H., Sheng, G.Y., He, K.B., and Fu, J.M.: Chemical  
13 characteristics of haze during summer and winter in Guangzhou, *Atmos. Res.*, 94, 238-245,  
14 <https://doi.org/10.1016/j.atmosres.2009.05.016>, 2009.
- 15 Tian, M., Wang, H., Chen, Y., Yang, F., Zhang, X., Zou, Q., Zhang, R., Ma, Y., and He, K.: Characteristics of aerosol  
16 pollution during heavy haze events in Suzhou, China. *Atmos. Chem. Phys.*, 16, 7357-7371,  
17 <https://doi.org/10.5194/acp-16-7357-2016>, 2016.
- 18 Torres, O., Ahn, C., and Chen, Z.: Improvements to the OMI near-UV aerosol algorithm using A-train CALIOP and  
19 AIRS observations, *Atmospheric Meas. Tech.*, 6, 3257-3270, <https://doi.org/10.5194/amt-6-3257-2013>,  
20 2013.
- 21 Vadrevu, K.P., Ellicott, E., Giglio, L., Badarinath, K.V.S., Vermote, E., Justice, C., and Lau, W.K.: Vegetation fires in  
22 the himalayan region—Aerosol load, black carbon emissions and smoke plume heights, *Atmos.*  
23 *Environ.*, 47, 241-251, <https://doi.org/10.1016/j.atmosenv.2011.11.009>, 2012.
- 24 Vakkari, V., Kerminen, V.M., Beukes, J.P., Tiitta, P., Zyl, P.G., Josipovic, M., Venter, A.D., Jaars, K., Worsnop, D.R.,  
25 Kulmala, M., and Laakso, L.: Rapid changes in biomass burning aerosols by atmospheric  
26 oxidation, *Geophys. Res. Lett.*, 41, 2644-2651, <https://doi.org/10.1002/2014GL059396>, 2014.
- 27 [Villalobos, A.M., Amonov, M.O., Shafer, M.M., Devi, J.J., Gupta, T., Tripathi, S.N., Rana, K.S., Mckenzie, M., Bergin,  
28 M.H. and Schauer, J.J.: Source apportionment of carbonaceous fine particulate matter \(PM<sub>2.5</sub>\) in two  
29 contrasting cities across the Indo-Gangetic plain, \*Atmos. Pollut. Res.\*, 6, 398-405,  
30 <https://doi.org/10.5094/APR.2015.044>, 2015.](https://doi.org/10.5094/APR.2015.044)
- 31 Wan, X., Kang, S., Li, Q., Rupakheti, D., Zhang, Q., Guo, J., Chen, P., Tripathi, L., Rupakheti, M., Panday, A.K.,  
32 and Wang, W.: Organic molecular tracers in the atmospheric aerosols from Lumbini, Nepal, in the  
33 northern Indo-Gangetic Plain: influence of biomass burning, *Atmos. Chem. Phys.*, 17, 8867-8885,  
34 <https://doi.org/10.5194/acp-17-8867-2017>, 2017.
- 35 Wang, Y., Hopke, P.K., Rattigan, O.V., Xia, X., Chalupa, D.C., and Utell, M.J.: Characterization of residential wood  
36 combustion particles using the two-wavelength aethalometer, *Environ. Sci. Technol.*, 45, 7387-7393,  
37 <http://doi.org/10.1021/es2013984>, 2011.
- 38 Wang, Y.Q., Zhang, X.Y., and Arimoto, R.: The contribution from distant dust sources to the atmospheric  
39 particulate matter loadings at XiAn, China during spring, *Sci. Total Environ.*, 368, 875-883,  
40 <https://doi.org/10.1016/j.scitotenv.2006.03.040>, 2006.
- 41 Wang, R., Balkanski, Y., Boucher, O., Bopp, L., Chappell, A., Ciais, P., Hauglustaine, D., Peñuelas, J. and Tao, S.:  
42 Sources, transport and deposition of iron in the global atmosphere, *Atmos. Chem. Phys.*, 15, 6247-  
43 6270, <https://doi.org/10.5194/acp-15-6247-2015>, 2015.

1 Zdrahal, Z., Oliveira, J., Vermeylen, R., Claeys, M., and Maenhaut, W.: Improved method for quantifying  
2 levoglucosan and related monosaccharide anhydrides in atmospheric aerosols and application to samples  
3 from urban and tropical locations, *Environ. Sci. Technol.*, 36, 747-753,  
4 <http://doi.org/10.1021/es015619v>, 2002.

5 Zhang, W., Tong, Y., Wang, H., Chen, L., Ou, L., Wang, X., Liu, G. and Zhu, Y.: Emission of metals from pelletized  
6 and uncompressed biomass fuels combustion in rural household stoves in China, *Sci. Rep.*, 4,  
7 5611, <https://doi.org/10.1038/srep05611>, 2014.

8



1 **List of figures:**

---

- 2 Fig. 1. Geographical location of aerosol ground monitoring station (a), and MODIS aerosol optical  
3 depth with NCEP/NCAR composite means of wind vector during monitoring period (b).
- 4 Fig. 2. Time series of (a) size segregated particulate mass concentration, (b) particle ratio and (c) daily  
5 means of meteorological variables.
- 6 Fig. 3. Variation of (a) ions and (b) trace metals in different aerosol size fractions.
- 7 Fig. 4. Variation of BC, Delta C and ABL during entire monitoring period.
- 8 Fig. 5. Size-segregated particulate bound (a) organic aerosols, and difference in the molecular  
9 compositions of (b) *n*-alkanes and (b) fatty acids.
- 10 Fig. 6. Temporal variation of trace gases and biomass burning signature molecules ( $\text{NH}_4^+$ ,  $\text{K}^+$ ,  
11 Levoglucosan), and their associations within different aerosol size fractions.
- 12 Fig. 7. Episode specific spatial distribution of AOD, AE, UVAI, surface CO (ppbv) and tropospheric  $\text{NO}_2$   
13 (molecules  $\text{cm}^{-2}$ ) over (a) South Asia and (b) at ground station.
- 14 Fig. 8. Aerosol vertical profiles from selected CALIPSO overpasses across ground station (a) aerosol  
15 subtypes, (b) extinction coefficients of each aerosol type and (c) time series of extinction profile  
16 for total and smoke aerosols.
- 17 Fig. 9. Episode specific MODIS fire count, fire radiative power (FRP, MW), brightness temperature (B.  
18 Temp., K), and five days air mass back-trajectory along with CWT.
- 19 Fig. 10. Episode specific aerosol short wave radiative forcing and atmospheric heating.

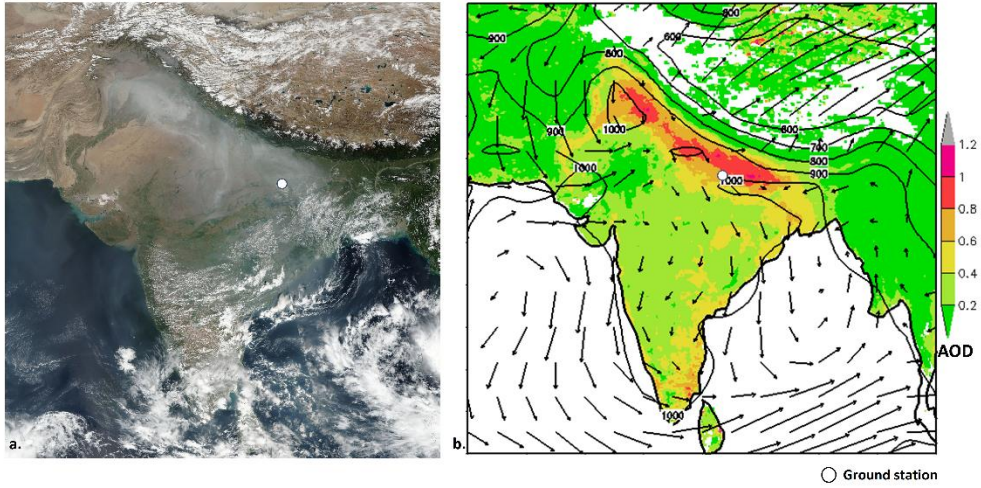
20

21

22

23

1  
2  
3

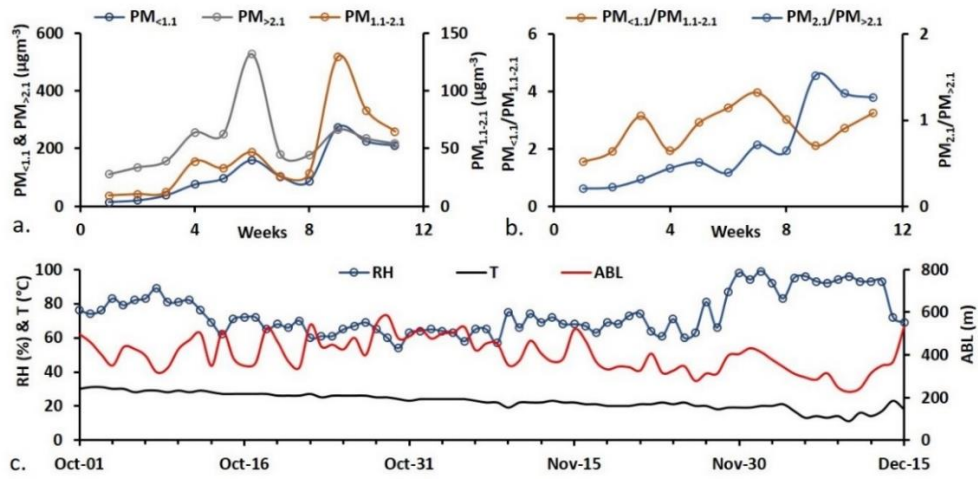


4  
5  
6  
7  
8  
9  
10

Fig. 1. Geographical location of aerosol ground monitoring station (a), and MODIS aerosol optical depth with NCEP/NCAR composite means of wind vector during monitoring period (b).

**Note:** Background image in (a) was retrieved from Suomi NPP VIIRS satellite indicating the thick aerosol layer over north India on October 31, 2016.

1



2

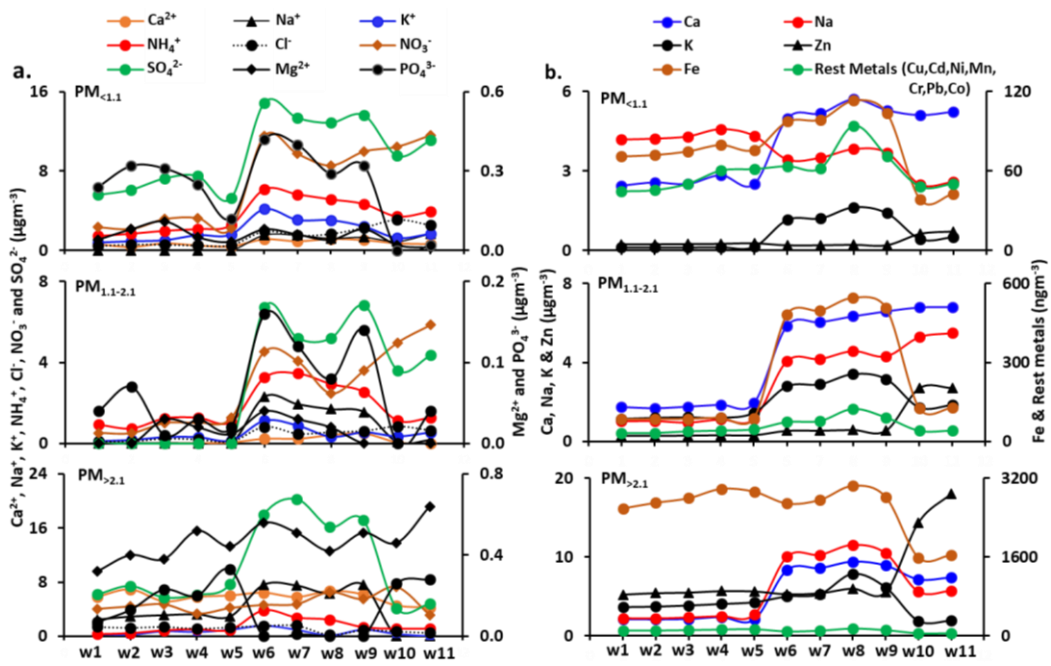
3 Fig. 2. Time series of (a) size segregated particulate mass concentration, (b) particle ratio and (c) daily  
4 means of meteorological variables.

5 **Note:** Week 1 to 5 are in the month of October, week 6 to 9 are in November and week 10 to 11 are  
6 in December.

7

8

1



2

3

4

Fig. 3. Variation of (a) ions and (b) trace metals in different aerosol size fractions.

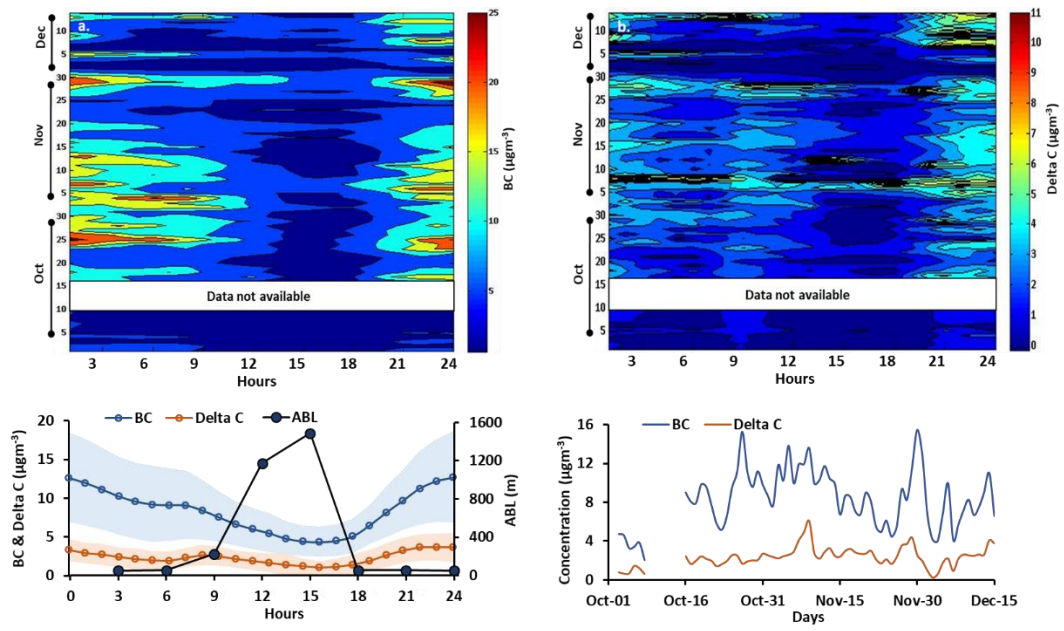
5

**Note:** Week 1 to 5 are in the month of October, week 6 to 9 are in November and week 10 to 11 are in December.

6

7

1  
2

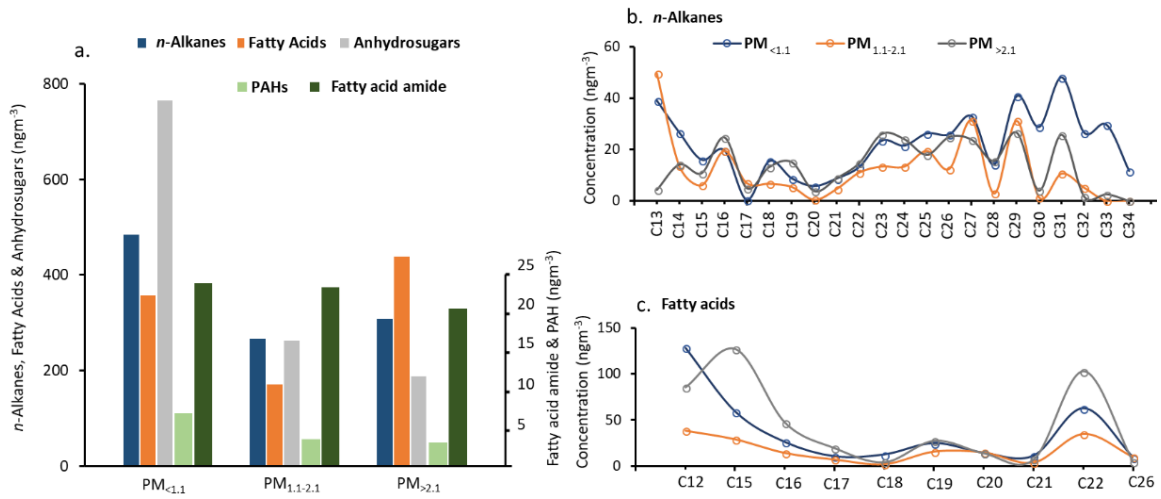


3  
4  
5  
6  
7  
8

Fig. 4. Variation of BC, Delta C and ABL during entire monitoring period.

**Note.** The blue and red shade in the graph at lower panel indicates the standard deviation.

1

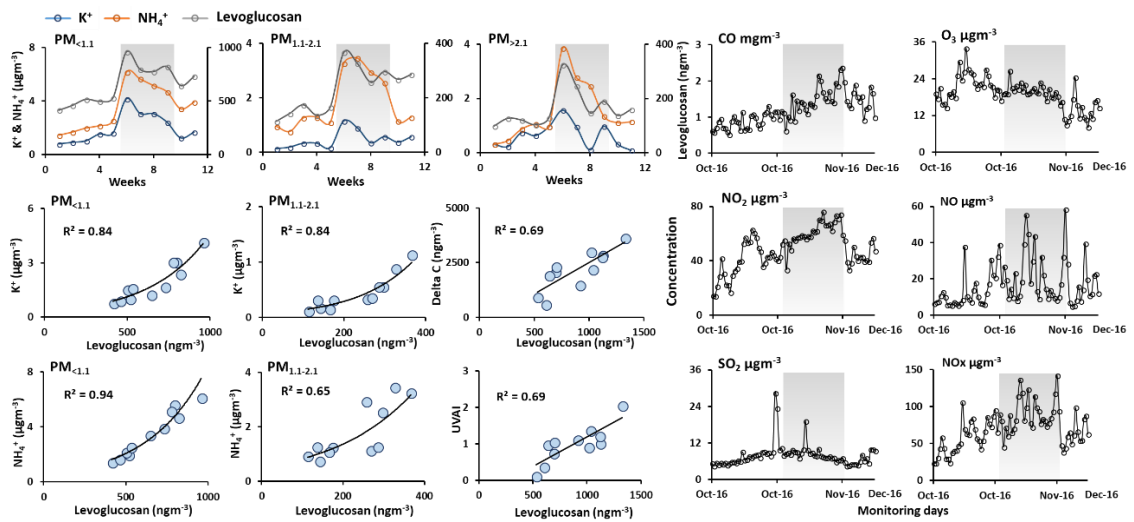


2  
3

4 Fig. 5. Size-segregated particulate bound (a) organic aerosols, and difference in the molecular  
5 compositions of (b) *n*-alkanes and (b) fatty acids.

6

1



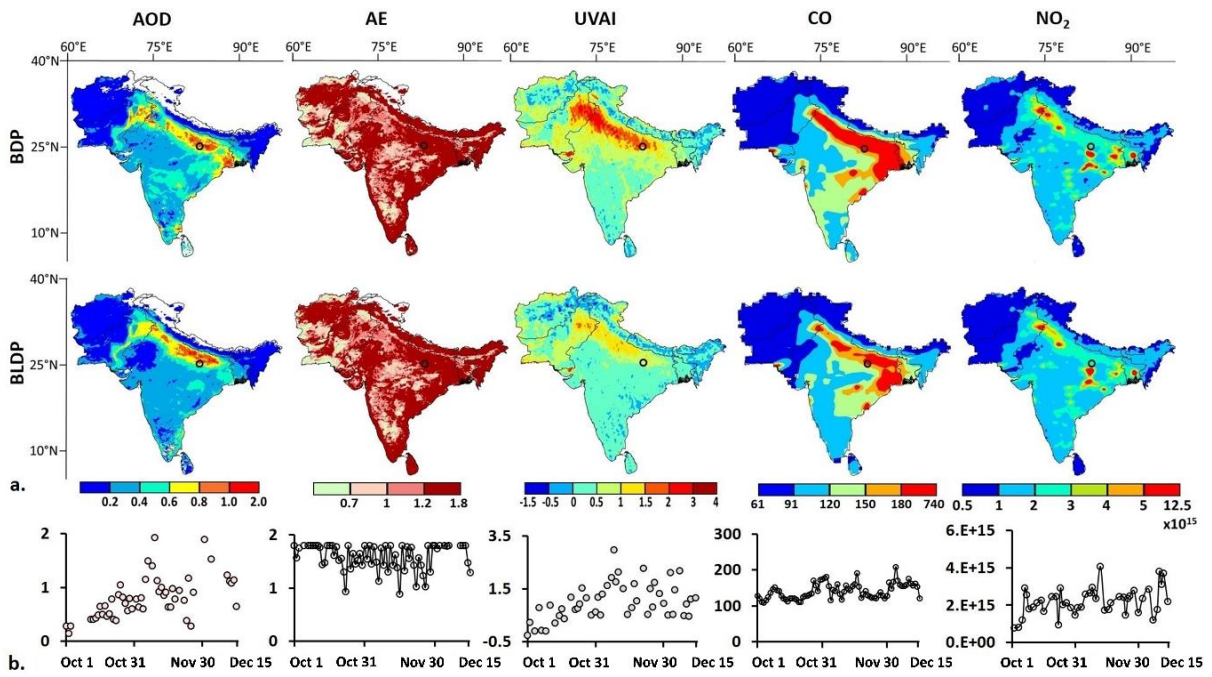
2

3

4 Fig. 6. Temporal variation of trace gases and biomass burning signature molecules ( $NH_4^+$ ,  $K^+$ ,  
5 Levoglucosan), and their associations within different aerosol size fractions.

6 **Note.** The shaded area indicates the peak biomass burning emissions.

1



2

3

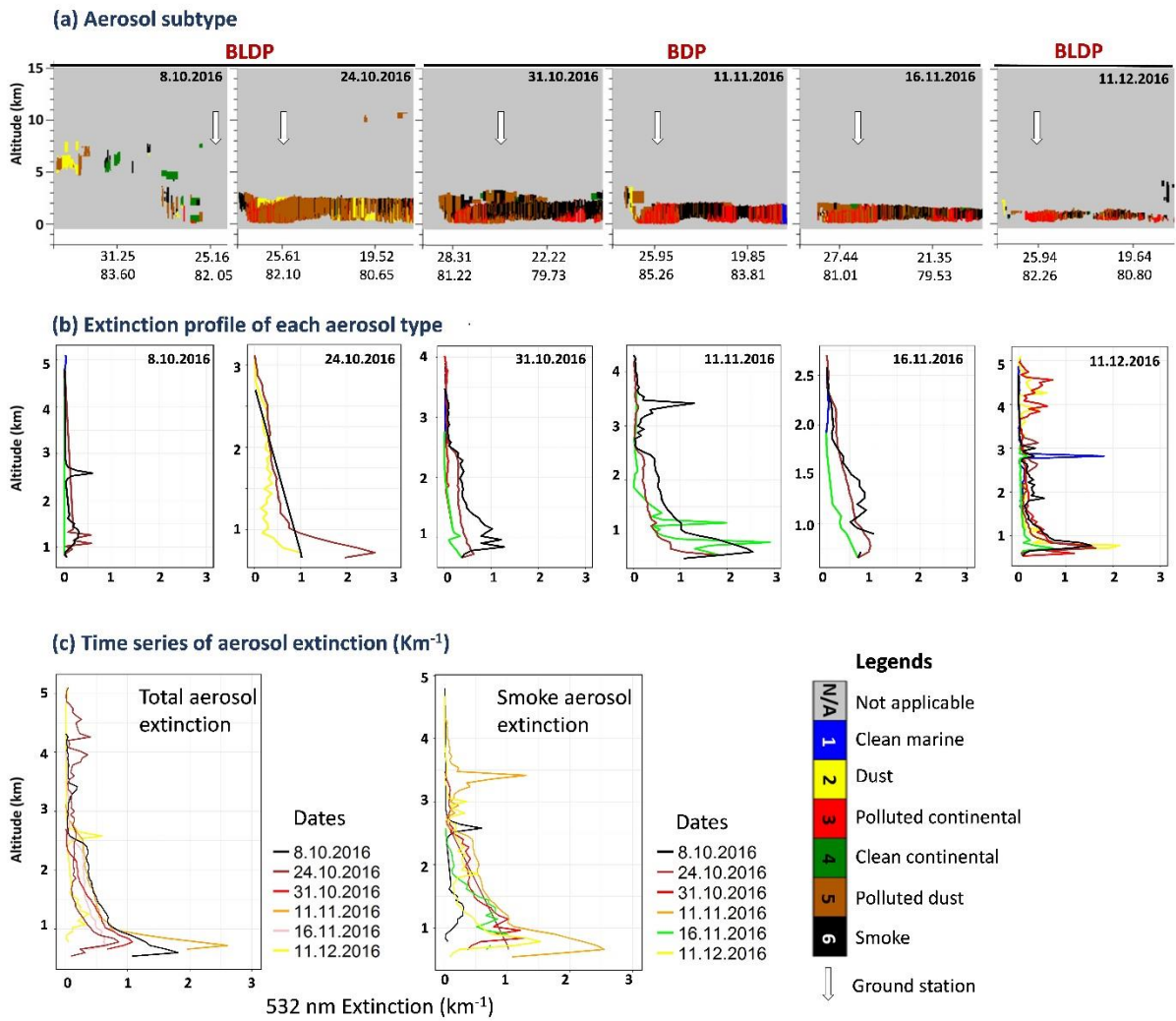
4 Fig. 7. Episode specific spatial distribution of AOD, AE, UVAI, surface CO (ppbv) and tropospheric NO<sub>2</sub>  
5 (molecules cm<sup>-2</sup>) over (a) South Asia and (b) at ground station.

6 **Note.** The lower panel indicates the time-series for each parameter retrieved particularly over the  
7 ground station.

8



1



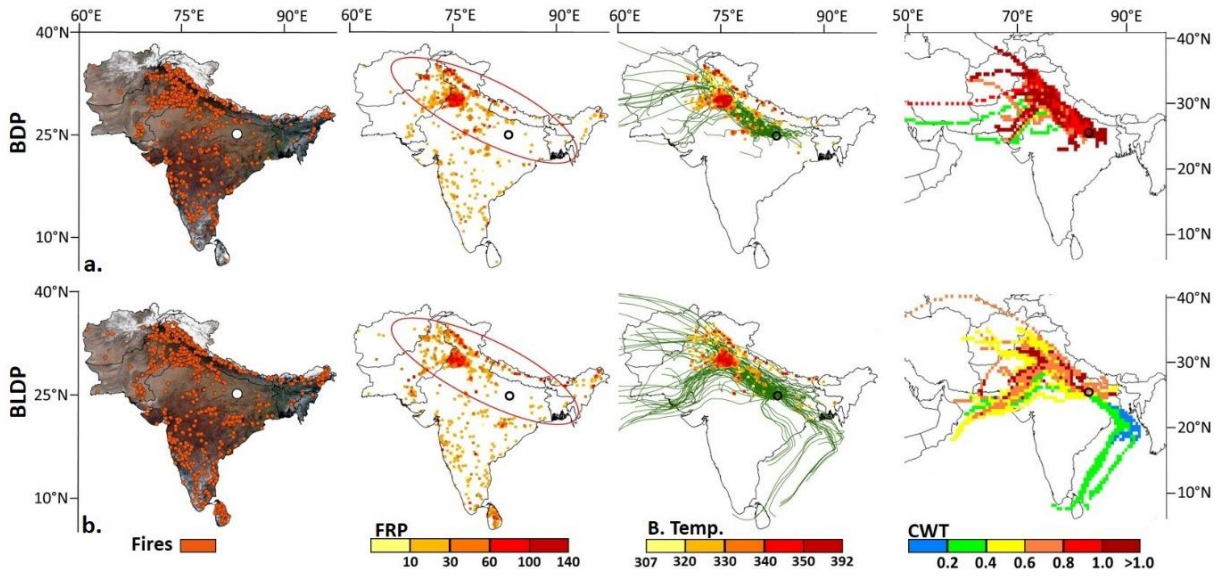
2

3

4 Fig. 8. Aerosol vertical profiles from selected CALIPSO overpasses across ground station (a) aerosol  
 5 subtypes, (b) extinction coefficients of each aerosol type and (c) time series of extinction  
 6 profile for total and smoke aerosols.

7

1



2

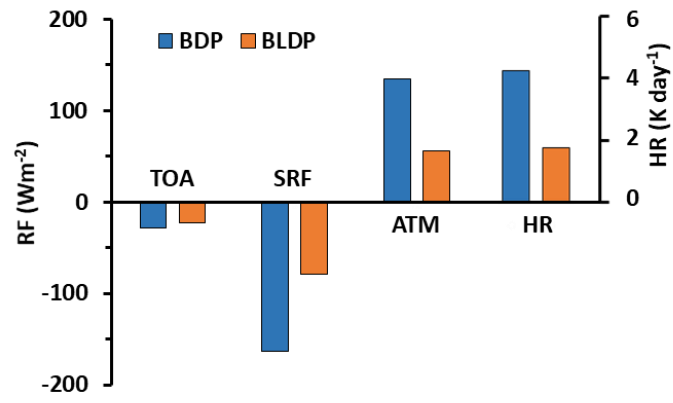
3

4 Fig. 9. Episode specific MODIS fire count, fire radiative power (FRP, MW), brightness temperature (B.  
5 Temp., K), and five days air mass back-trajectory along with CWT.

6

7

1



2

3

4

Fig. 10. Episode specific aerosol short wave radiative forcing and atmospheric heating.

5

6